FINAL TECHNICAL REPORT ON NAG7-871

DEVELOPMENT OF FAST ALGORITHMS USING RECURSION, NESTING AND ITERATIONS FOR COMPUTATIONAL ELECTROMAGNETICS

W. C. Chew, J.M. Song, C. C. Lu, and W. H. Weedon
Electromagnetics Laboratory
Department of Electrical and Computer Engineering
University of Illinois
Urbana, IL 61801

Abstract

In the first phase of our work, we have concentrated on laying the foundation to develop fast algorithms. We have developed some basic codes for three-dimensional scattering and studied several candidate algorithms for speeding up the codes. These algorithms include using recursive structure like the recursive aggregate interaction matrix algorithm (RAIMA), the nested equivalence principle algorithm (NEPAL), the ray-propagation fast multipole algorithm (RPFMA), and the multi-level fast multipole algorithm (MLFMA). We have also investigated the use of curvilinear patches to build a basic method of moments code where these acceleration techniques can be used later.

In the second phase of our work, we have concentrated on implementing three-dimensional NEPAL on a massively parallel machine, the Connection Machine CM-5. We have been able obtain some 3D scattering result on the Connection Machine, CM-5. In order to understand the parallelization of codes on the Connection Machine, we have also studied the parallelization of 3D finite-difference time-domain (FDTD) code with PML material absorbing boundary condition (ABC). We found that simple algorithms like the FDTD with material ABC can be parallelized very well allowing us to solve over a-million-node problem under one minute. In addition to the above, we have studied the use of the fast multipole method and the ray-propagation fast multipole algorithm to expedite matrix-vector multiply in a conjugate-gradient solution to integral equation of scattering. We find that these methods are faster than LU decomposition for one incident angle, but are slower than LU decomposition when many incident angles are needed as in the monostatic RCS calculations.

CHAPTER 1

NESTED EQUIVALENCE PRINCIPAL ALGORIHTM (NEPAL) IN THREE DIMENSIONS

1. Introduction

The computation of electromagnetic scattering of three dimensional objects finds applications in many areas. Hence, it has been earnestly studied by many engineers, scientists and mathematicians alike. As a result, many algorithms have been developed for solving 3D scattering problems. Among these algorithms, finite difference time domain methods are popular due to their lower complexity and ease of implementations. However, many of these methods are for one excitation only, and the solution process needs to be repeated for multiple excitations. Moreover, absorbing boundary conditions are required for those algorithms. On the other hand, the solution to integral equations automatically satisfies the radiation condition. As a result, an integral equation solver with computational complexity comparable to differential equation solvers is a viable alternative solution technique to these scattering problems.

This paper presents an integral equation solver using the nested equivalence principle algorithm (NEPAL) which has been successfully applied to 2D problems [1]. It is known that in solving an integral equation, one can first replace the volume scatterer by small subscatterers where the size of a subscatterer is much smaller than a wavelength. The unknown function to be sought is expanded in terms of basis functions which usually have their supports on the subscatterers. By matching the field on the subscatterers, a set of linear equations are formed. The number of unknowns is proportional to the number of subscatterers in this case. Physically, each subscatterer can be considered a scattering center.

The interaction of a subscatterer with the other subscatterers can be described by interaction matrices [9]. If there are N subscatterers, then there will be N^2 interaction matrices since each subscatterer will interact with all the other subscatterers including itself. The N^2 interaction matrices can be found with N^3 operations [8,9]. The idea of NEPAL is to reduce the number of scattering centers, and hence to reduce the CPU time required for the solution.

Similar algorithms for inversion of a matrix using nested dissection method for the finite element method can be found in [10]. It is shown in [1] that the computational complexity of NEPAL is asymptotically $N^{1.5}$ for 2D problems. In this paper, we will first formulate NEPAL for three dimensional problems and show that the complexity in 3D is N^2. In addition, we will use some of the symbols differently. For example, i is used either as a summation index or as the imaginary number $\sqrt{-1}$. The meaning is clear from the context.

2. Formulation of the Problem

A three dimensional volume can be discretized into a set of small cubic boxes called subscatterers. Each subscatterer has volume Δ^3. The scattering property of each subscatterer can be represented by a multipole with order proportional to the electrical size of the subscatterer. The scattered field can be written as [2],

$$\begin{aligned}\mathbf{E}(\mathbf{r}) &= \sum_{nm} \left\{ \mathbf{M}_{nm}(\mathbf{r}-\mathbf{r}_i) \left[\mathbf{b}_i^M\right]_{nm} + \mathbf{N}_{nm}(\mathbf{r}-\mathbf{r}_i) \left[\mathbf{b}_i^E\right]_{nm} \right\} \\ &= \overline{\psi}^t(\mathbf{r}-\mathbf{r}_i)\cdot\mathbf{b}_i, \end{aligned} \tag{1}$$

where, $\mathbf{b}_i = \left[\mathbf{b}_i^M, \mathbf{b}_i^E\right]^t$ is the multipole coefficients, superscript M stands for TE component, and E for TM component. Here, $\overline{\psi}^t(\mathbf{r}) = [\mathbf{M}, \mathbf{N}]$ is the vector spherical wave function, and $\mathbf{M}$ and $\mathbf{N}$ are given by [2,4]

$$\mathbf{M}_{nm}(\mathbf{r}) = \hat{\theta}\frac{im}{\sin\theta} z_n(kr) Y_{nm}(\theta,\phi) - \hat{\phi} z_n(kr) \frac{\partial Y_{nm}(\theta,\phi)}{\partial\theta},$$

$$\begin{aligned}\mathbf{N}_{nm}(\mathbf{r}) =& \hat{r}\frac{n(n+1)}{kr} z_n(kr) Y_{nm}(\theta,\phi) + \hat{\theta}\frac{1}{kr}\frac{\partial}{\partial r}\left[r z_n(kr)\right]\frac{\partial Y_{nm}(\theta,\phi)}{\partial\theta} \\ &+ \hat{\phi}\frac{im}{kr\sin\theta}\frac{\partial}{\partial r}\left[r z_n(kr)\right] Y_{nm}(\theta,\phi).\end{aligned}$$

$$n = 1, 2, \cdots, \quad m = -n, \cdots, n.$$

In the above, $z_n(kr)$ is a spherical Bessel function or spherical Hankel function of the first kind depending on whether $\overline{\psi}^t(\mathbf{r})$ is an incoming wave or an outgoing wave, respectively. When Bessel function is used, $\Re g\overline{\psi}$, means the regular part of $\overline{\psi}$, which replaces $\overline{\psi}$. In the above, Y_{nm} is a spherical harmonic, and it is defined by [4]

$$Y_{nm}(\theta,\phi) = (-1)^m \sqrt{\frac{2n+1}{4\pi}\frac{(n-m)!}{(n+m)!}} P_n^m(\cos\theta) e^{im\phi}, \qquad m \geq 0,$$

$$Y_{nm}(\theta,\phi) = (-1)^{|m|} Y_{n|m|}(\theta,\phi), \qquad m < 0,$$

where, P_n^m is the associated Legendre function.

Expressing the incident field in the same manner,

$$\mathbf{E}^{inc}(\mathbf{r}) = \Re g \overline{\psi}^t(\mathbf{r} - \mathbf{r}_i) \cdot \overline{\alpha}_{is} \cdot \mathbf{a}_s, \tag{2}$$

we can relate the unknown coefficient $\mathbf{b}_i$ to $\mathbf{a}_s$ via a T-matrix by matching the field on the boundary of the subscatterer [2,6,7]:

$$\mathbf{b}_i = \overline{\mathbf{T}} \cdot \overline{\alpha}_{is} \cdot \mathbf{a}_s. \tag{3}$$

In the above, $\overline{\alpha}_{is}$ is a translation matrix [2,5], and $\mathbf{a}_s$ is the incident wave amplitude.

When Δ is small, the T-matrix is diagonal and close to that of a sphere, and can be found using the Mie series [2]. When N_A subscatterers are present, the coefficients $\mathbf{b}_i$ will be unknown which satisfy the following brute force equations [11,12]:

$$\mathbf{b}_i = \overline{\mathbf{T}}_i \cdot \left[\overline{\alpha}_{is} \cdot \mathbf{a}_s + \sum_{\substack{j=1 \\ j \neq i}}^{N_A} \overline{\alpha}_{ij} \cdot \mathbf{b}_j \right], \qquad i = 1, 2, \cdots, N_A. \tag{4}$$

The solution to the above equations can be written as

$$\mathbf{b}_i = \sum_{j=1}^{N_A} \overline{\mathbf{I}}_{ij(N_A)} \cdot \overline{\alpha}_{js} \cdot \mathbf{a}_s, \qquad i = 1, 2, \cdots, N_A. \tag{5}$$

Hence, the scattered field is given by

$$\mathbf{E}^{sca}(\mathbf{r}) = \sum_{i=1}^{N_A} \overline{\psi}^t(\mathbf{r} - \mathbf{r}_i) \cdot \sum_{j=1}^{N_A} \overline{\mathbf{I}}_{ij(N_A)} \cdot \overline{\alpha}_{js} \cdot \mathbf{a}_s. \tag{6}$$

In the above, $\overline{\mathbf{I}}_{ij(N_A)}$, $i, j = 1, 2, \cdots, N_A$ are called interaction matrices; they describe the interactions between N_A subscatterers. They can be found in a variety of ways, for example, by Gaussian elimination, or by a recursive algorithm [8,9].

3. Equivalence of Interaction Matrices.

As shown in the above section, the scattered field can be determined by the N_A^2 interaction matrices for a group of N_A subscatterers. In this section,

Definition : Two sets of interaction matrices $\bar{\mathbf{I}}_{ij(N_A)}$ and $\bar{\mathbf{I}}_{ij(N_B)}$ are said to be equivalent if they generate the same scattered field via Equation (6) for the same incident field.

we will show that there is another set of interaction matrices which will generate the same scattered field. To this end, we first give a definition of equivalent interaction matrices.

In the following, we will give a mathematical description for the equivalence of the interior subscatterer by those on the surface using Huygens' equivalence principle [3].

First, we assume that S is the boundary of a volume region V, and V contains sources which generate field $\mathbf{E}$ and $\mathbf{H}$ on the boundary. Next, we let $\mathbf{r}'$ be a point outside V, as shown in Figure 1. Huygens' equivalence principle states that the field at $\mathbf{r}'$ due to sources inside V can be represented via equivalent sources on the boundary:

$$\mathbf{E}(\mathbf{r}') = -\oint_S dS \left[\hat{n} \times \mathbf{E}(\mathbf{r}) \cdot \nabla \times \overline{\mathbf{G}}_e(\mathbf{r}, \mathbf{r}') + i\omega\mu\hat{n} \times \mathbf{H}(\mathbf{r}) \cdot \overline{\mathbf{G}}_e(\mathbf{r}, \mathbf{r}')\right], \quad (7)$$

where,

$$\overline{\mathbf{G}}_e(\mathbf{r}, \mathbf{r}') = \left(\bar{\mathbf{I}} + \frac{\nabla\nabla}{k^2}\right) \frac{e^{ik|\mathbf{r}-\mathbf{r}'|}}{4\pi|\mathbf{r}-\mathbf{r}'|} \quad (7a)$$

is the free space dyadic Green's function. Equation (7) has a double roles. First of all, it provides an indirect approach to compute the field at points outside V. Secondly, it tells us how to construct the equivalent sources: the equivalent sources are simply the tangential components of the fields.

Apart from the above two points, we also observed that: (1) The equivalence principle does not specify the type and the number of the original sources inside V; they can be induced sources, or even some other equivalent sources. Also, there could be only one point source, more than one point source or distributed sources. (2) The equivalent sources are uniquely determined by the shape of the surface and the density of the tangential field components. This gives us the possibility of replacing a large number of sources with a relatively small number of sources.

The mathematical representation of a source can be different. For example, Equation (2) represents a direct source by its multipole amplitude, while Equation (6) represents the induced sources by a set of matrices $\bar{\mathbf{I}}_{ij(N_A)}$, $i, j = 1, 2, \cdots, N_A$. Similarly, we can represent the equivalent sources in the same

manner, i.e., another set of interaction matrices $\bar{\mathbf{I}}_{ij(N_B)}, i, j = 1, 2, \cdots, N_B$. We now construct the relation between the two sets of matrices using Equation (7).

First, we divide the surface S into N_B small surfaces or patches, where each patch is of area ΔS. As a result, Equation (7) can be rewritten as

$$\mathbf{E}(\mathbf{r}') = -\sum_{i=1}^{N_B} \int_{\Delta S_i} dS \left[\hat{n} \times \mathbf{E}(\mathbf{r}) \cdot \nabla \times \overline{\mathbf{G}}_e(\mathbf{r}, \mathbf{r}') + i\omega\mu\hat{n} \times \mathbf{H}(\mathbf{r}) \cdot \overline{\mathbf{G}}_e(\mathbf{r}, \mathbf{r}')\right]. \tag{8}$$

At the i-th patch, we let $\mathbf{r} = \mathbf{r}'' + \mathbf{r}_i$. Here, $\mathbf{r}''$ is the local coordinate for the i-th patch. Then,

$$\mathbf{r} - \mathbf{r}' = \mathbf{r}'' + \mathbf{r}_i - \mathbf{r}' = \mathbf{r}'' - (\mathbf{r}' - \mathbf{r}_i). \tag{9}$$

Under the condition that $|\mathbf{r}' - \mathbf{r}_i| > |\mathbf{r}''|$, the Green's function $\overline{\mathbf{G}}_e(\mathbf{r}, \mathbf{r}')$ can be expanded as ($\mathbf{r}_i' = \mathbf{r}' - \mathbf{r}_i$, [3, p.409])

$$\overline{\mathbf{G}}_e(\mathbf{r}'', \mathbf{r}_i') = \sum_{nm} \frac{ik(-)^m}{n(n+1)} \left[\Re g \mathbf{M}_{n,-m}(\mathbf{r}'')\mathbf{M}_{nm}(\mathbf{r}_i') + \Re g \mathbf{N}_{n,-m}(\mathbf{r}'')\mathbf{N}_{nm}(\mathbf{r}_i')\right]. \tag{10}$$

When this expansion is applied to Equation (8), we have

$$\begin{aligned}\mathbf{E}(\mathbf{r}') = \sum_{i,nm} \frac{-ik^2(-)^m}{n(n+1)} \int_{\Delta S_i} dS'' \Big[&\hat{n} \times \mathbf{E}(\mathbf{r}) \cdot \Re g \mathbf{N}_{n,-m}(\mathbf{r}'')\mathbf{M}_{nm}(\mathbf{r}_i') \\ &+\hat{n} \times \mathbf{E}(\mathbf{r}) \cdot \Re g \mathbf{M}_{n,-m}(\mathbf{r}'')\mathbf{N}_{nm}(\mathbf{r}_i') \\ &+i\eta\hat{n} \times \mathbf{H}(\mathbf{r}) \cdot \Re g \mathbf{M}_{n,-m}(\mathbf{r}'')\mathbf{M}_{nm}(\mathbf{r}_i') \\ &+i\eta\hat{n} \times \mathbf{H}(\mathbf{r}) \cdot \Re g \mathbf{N}_{n,-m}(\mathbf{r}'')\mathbf{N}_{nm}(\mathbf{r}_i')\Big], \end{aligned} \tag{11}$$

where, $\eta = \sqrt{\mu_0/\epsilon_0}$ is the free space impedance.

Equation (11) can be written more compactly as

$$\mathbf{E}(\mathbf{r}') = \sum_i \sum_{nm} \left\{\mathbf{M}_{nm}(\mathbf{r}_i') \cdot [\mathbf{b}_i^M]_{nm} + \mathbf{N}_{nm}(\mathbf{r}_i') \cdot [\mathbf{b}_i^E]_{nm}\right\}, \tag{12}$$

where, upon making approximations to the integrals,

$$[\mathbf{b}_i^M]_{nm} = \frac{-ik^2(-)^m}{n(n+1)} \Delta S \Big[\hat{n}_i \times \mathbf{E}(\mathbf{r}_i) \cdot \Re g \mathbf{N}_{n,-m}(0)\Big], \tag{13a}$$

$$[\mathbf{b}_i^E]_{nm} = \frac{-ik^2(-)^m}{n(n+1)}\Delta S\Big[i\eta\hat{n}_i \times \mathbf{H}(\mathbf{r}_i)\cdot \Re g\mathbf{N}_{n,-m}(0)\Big], \qquad (13b)$$

where, $\hat{n}_i$ is the average normal of the i-th patch.

In deriving Equation (11), the identities

$$\nabla \times \mathbf{M} = k\mathbf{N}, \qquad \nabla \times \mathbf{N} = k\mathbf{M}$$

have been used. Equation (12) gives the source-field relation for the equivalent sources on the surface S.

We assume that the source-field relation for the interior sources is of the form as Equation (1) with multipole amplitude given by $\mathbf{a}_j$, $j = 1, 2, ..., N_A$. Then,

$$\mathbf{E}(\mathbf{r}) = \sum_{j,\nu\mu}\Big\{\mathbf{M}_{\nu\mu}(\mathbf{r}-\mathbf{r}_j)\cdot[\mathbf{a}_j^M]_{\nu\mu} + \mathbf{N}_{\nu\mu}(\mathbf{r}-\mathbf{r}_j)\cdot[\mathbf{a}_j^E]_{\nu\mu}\Big\}, \qquad (14a)$$

$$\mathbf{H}(\mathbf{r}) = \frac{1}{i\eta}\sum_{j,\nu\mu}\Big\{\mathbf{N}_{\nu\mu}(\mathbf{r}-\mathbf{r}_j)\cdot[\mathbf{a}_j^M]_{\nu\mu} + \mathbf{M}_{\nu\mu}(\mathbf{r}-\mathbf{r}_j)\cdot[\mathbf{a}_j^E]_{\nu\mu}\Big\}. \qquad (14b)$$

We let $\mathbf{r} = \mathbf{r}_i$ in Equations (14a) and (14b), and substitute them into Equation (13a), we have

$$\begin{aligned}[\mathbf{b}_i^M]_{nm} =& \frac{-ik^2(-)^m}{n(n+1)}\Delta S\Re g\mathbf{N}_{n,-m}(0) \\ & \cdot\sum_{j,\nu\mu}\Big(\hat{n}_i\times\mathbf{M}_{\nu\mu}(\mathbf{r}_{ji})\cdot[\mathbf{a}_j^M]_{\nu\mu} + \hat{n}_i\times\mathbf{N}_{\nu\mu}(\mathbf{r}_{ji})\cdot[\mathbf{a}_j^E]_{\nu\mu}\Big),\end{aligned}$$

or

$$[\mathbf{b}_i^M]_{nm} = \sum_{j,\nu\mu}\left\{[\bar{\mathbf{c}}_{ij}^{MM}]_{nm,\nu\mu}\cdot[\mathbf{a}_j^M]_{\nu\mu} + [\bar{\mathbf{c}}_{ij}^{ME}]_{nm,\nu\mu}\cdot[\mathbf{a}_j^E]_{\nu\mu}\right\}. \qquad (15a)$$

Similarly,

$$[\mathbf{b}_i^E]_{nm} = \sum_{j,\nu\mu}\left\{[\bar{\mathbf{c}}_{ij}^{EM}]_{nm,\nu\mu}\cdot[\mathbf{a}_j^M]_{\nu\mu} + [\bar{\mathbf{c}}_{ij}^{EE}]_{nm,\nu\mu}\cdot[\mathbf{a}_j^E]_{\nu\mu}\right\}, \qquad (15b)$$

where, $\mathbf{r}_{ji} = \mathbf{r}_i - \mathbf{r}_j$ and

$$[\bar{\mathbf{c}}_{ij}^{MM}]_{nm,\nu\mu} = \frac{-ik^2(-)^m}{n(n+1)}\Delta S\Re g\mathbf{N}_{n,-m}(0)\cdot\hat{n}_i\times\mathbf{M}_{\nu\mu}(\mathbf{r}_{ji}), \qquad (16a)$$

$$[\bar{\mathbf{c}}_{ij}^{ME}]_{nm,\nu\mu} = \frac{-ik^2(-)^m}{n(n+1)}\Delta S\Re g\mathbf{N}_{n,-m}(0)\cdot\hat{n}_i\times\mathbf{N}_{\nu\mu}(\mathbf{r}_{ji}), \qquad (16b)$$

$$[\overline{\mathbf{c}}_{ij}^{EM}]_{nm,\nu\mu} = [\overline{\mathbf{c}}_{ij}^{ME}]_{nm,\nu\mu}, \tag{16c}$$

$$[\overline{\mathbf{c}}_{ij}^{EE}]_{nm,\nu\mu} = [\overline{\mathbf{c}}_{ij}^{MM}]_{nm,\nu\mu}. \tag{16d}$$

Denoting

$$\overline{\mathbf{h}}_{ij}^{(o)} = \overline{\mathbf{c}}_{ij} = \begin{bmatrix} \overline{\mathbf{c}}_{ij}^{MM} & \overline{\mathbf{c}}_{ij}^{ME} \\ \overline{\mathbf{c}}_{ij}^{EM} & \overline{\mathbf{c}}_{ij}^{EE} \end{bmatrix},$$

we have the relation between the equivalent sources and the original sources:

$$\mathbf{b}_i = \sum_j \overline{\mathbf{h}}_{ij}^{(o)} \cdot \mathbf{a}_j,$$

where $\mathbf{b}_i = [\mathbf{b}_i^M, \mathbf{b}_i^E]^t$ and $\mathbf{a}_j = [\mathbf{a}_j^M, \mathbf{a}_j^E]^t$. If there is only one interior source located at $\mathbf{r}_j$ inside V, then the field at $\mathbf{r}'$ corresponding to this source is given by (14a) with $N_A = 1$, or

$$\mathbf{E}(\mathbf{r}') = \overline{\boldsymbol{\psi}}^t(\mathbf{r}' - \mathbf{r}_j) \cdot \mathbf{a}_j.$$

This is the direct source-field relation. On the other hand, we have an indirect source-field relation as Equation (12), or

$$\mathbf{E}(\mathbf{r}') = \sum_{i=1}^{N_B} \overline{\boldsymbol{\psi}}^t(\mathbf{r}' - \mathbf{r}_i) \cdot \overline{\mathbf{h}}_{ij}^{(o)} \cdot \mathbf{a}_j.$$

Equating the two representations, we have for arbitrary $\mathbf{a}_j$,

$$\overline{\boldsymbol{\psi}}^t(\mathbf{r} - \mathbf{r}_j) = \sum_{i=1}^{N_B} \overline{\boldsymbol{\psi}}^t(\mathbf{r} - \mathbf{r}_i) \cdot \overline{\mathbf{h}}_{ij}^{(o)}. \tag{17}$$

Equation (17) is the first equation which will be used in deriving the equivalence between interaction matrices of interior subscatterers and boundary subscatterers.

Now we consider the reverse problem: the sources are outside of V and we need to compute the field at $\mathbf{r}'$ inside V due to the outside sources.

Using the similar steps as in deriving $\overline{\mathbf{h}}_{ii'}^{(o)}$, we can write the field $\mathbf{E}(\mathbf{r}')$ in the same form as Equations (12), (13a) and (13b), except that $\mathbf{r}'$ is insider V in this case.

Suppose that the source is located at $\mathbf{r}_s$ and the multipole amplitude $\mathbf{a}_s$ for the source are known, then the fields at $\mathbf{r}$ due to this source are given by

$$\mathbf{E}(\mathbf{r}) = \sum_{\nu\mu} \Big\{ \mathbf{M}_{\nu\mu}(\mathbf{r}-\mathbf{r}_s) \cdot [\mathbf{a}_s^M]_{\nu\mu} + \mathbf{N}_{\nu\mu}(\mathbf{r}-\mathbf{r}_s) \cdot [\mathbf{a}_s^E]_{\nu\mu} \Big\}, \tag{18a}$$

$$\mathbf{H}(\mathbf{r}) = \frac{1}{i\eta} \sum_{\nu\mu} \Big\{ \mathbf{N}_{\nu\mu}(\mathbf{r}-\mathbf{r}_s) \cdot [\mathbf{a}_s^M]_{\nu\mu} + \mathbf{M}_{\nu\mu}(\mathbf{r}-\mathbf{r}_s) \cdot [\mathbf{a}_s^E]_{\nu\mu} \Big\}. \tag{18b}$$

Equation (18) gives an outgoing wave centered at $\mathbf{r}_s$, and the field point $\mathbf{r}$ is not specified yet. Now, we let $\mathbf{r}$ be a point in the vicinity of $\mathbf{r}_i \in S$, with $i = 1, 2, ..., N_B$. Observe that at $\mathbf{r}$, the field can also be considered incoming waves centered at $\mathbf{r}_i$. This is more rigorously given by the wave translation equation[4,5]:

$$\mathbf{M}(\mathbf{r}-\mathbf{r}_s) = \Re g\mathbf{M}(\mathbf{r}-\mathbf{r}_i) \cdot \overline{\mathbf{A}}_{is} + \Re g\mathbf{N}(\mathbf{r}-\mathbf{r}_i) \cdot \overline{\mathbf{B}}_{is},$$
$$\mathbf{N}(\mathbf{r}-\mathbf{r}_s) = \Re g\mathbf{M}(\mathbf{r}-\mathbf{r}_i) \cdot \overline{\mathbf{B}}_{is} + \Re g\mathbf{N}(\mathbf{r}-\mathbf{r}_i) \cdot \overline{\mathbf{A}}_{is}.$$

Therefore,

$$\mathbf{E}(\mathbf{r}) = \sum_{\nu\mu} \Big\{ \Re g\mathbf{M}_{\nu\mu}(\mathbf{r}-\mathbf{r}_i) \cdot [\mathbf{a}_{is}^M]_{\nu\mu} + \Re g\mathbf{N}_{\nu\mu}(\mathbf{r}-\mathbf{r}_i) \cdot [\mathbf{a}_{is}^E]_{\nu\mu} \Big\}, \tag{18c}$$

$$\mathbf{H}(\mathbf{r}) = \frac{1}{i\eta} \sum_{\nu\mu} \Big\{ \Re g\mathbf{N}_{\nu\mu}(\mathbf{r}-\mathbf{r}_i) \cdot [\mathbf{a}_{is}^M]_{\nu\mu} + \Re g\mathbf{M}_{\nu\mu}(\mathbf{r}-\mathbf{r}_i) \cdot [\mathbf{a}_{is}^E]_{\nu\mu} \Big\}, \tag{18d}$$

where, $\mathbf{a}_{is}$ is related to $\mathbf{a}_s$ by

$$\mathbf{a}_{is} = \begin{bmatrix} \overline{\mathbf{A}}_{is} & \overline{\mathbf{B}}_{is} \\ \overline{\mathbf{B}}_{is} & \overline{\mathbf{A}}_{is} \end{bmatrix} \cdot \mathbf{a}_s = \overline{\alpha}_{is} \cdot \mathbf{a}_s.$$

Substitution of (18c) and (18d) into Equation (13a), we have

$$[\mathbf{b}_i^M]_{nm} = \frac{-ik^2(-)^m}{n(n+1)} \Delta S \Re_g \mathbf{N}_{n,-m}(0)$$
$$\cdot \hat{n}_i \times \sum_{\nu\mu} \Big(\Re g\mathbf{M}_{\nu\mu}(0) \cdot [\mathbf{a}_{is}^M]_{\nu\mu} + \Re g\mathbf{N}_{\nu\mu}(0) \cdot [\mathbf{a}_{is}^E]_{\nu\mu} \Big),$$

or

$$[\mathbf{b}_i^M]_{nm} = \sum_{\nu\mu} \left\{ [\mathbf{c}_i^{MM}]_{nm,\nu\mu} \cdot [\mathbf{a}_{is}^M]_{\nu\mu} + [\mathbf{c}_i^{ME}]_{nm,\nu\mu} \cdot [\mathbf{a}_{is}^E]_{\nu\mu} \right\}. \tag{19a}$$

Similarly,

$$[\mathbf{b}_i^E]_{nm} = \sum_{\nu\mu} \left\{ [\mathbf{c}_i^{EM}]_{nm,\nu\mu} \cdot [\mathbf{a}_{is}^M]_{\nu\mu} + [\mathbf{c}_i^{EE}]_{nm,\nu\mu} \cdot [\mathbf{a}_{is}^E]_{\nu\mu} \right\}. \tag{19b}$$

Hence,

$$\mathbf{b}_i = \overline{\mathbf{c}}_i \cdot \mathbf{a}_s = \begin{bmatrix} \overline{\mathbf{c}}_i^{MM} & \overline{\mathbf{c}}_i^{ME} \\ \overline{\mathbf{c}}_i^{ME} & \overline{\mathbf{c}}_i^{EE} \end{bmatrix} \cdot \mathbf{a}_{is}, \tag{19c}$$

where,

$$[\mathbf{c}_i^{MM}]_{nm,\nu\mu} = \frac{-ik^2(-)^m}{n(n+1)} \Delta S \Re g \mathbf{N}_{n,-m}(0) \cdot \hat{n}_i \times \Re g \mathbf{M}_{\nu\mu}(0), \tag{20a}$$

$$[\mathbf{c}_i^{ME}]_{nm,\nu\mu} = \frac{-ik^2(-)^m}{n(n+1)} \Delta S \Re g \mathbf{N}_{n,-m}(0) \cdot \hat{n}_i \times \Re g \mathbf{N}_{\nu\mu}(0), \tag{20b}$$

$$[\mathbf{c}_i^{EM}]_{nm,\nu\mu} = [\mathbf{c}_i^{ME}]_{nm,\nu\mu}, \tag{20c}$$

$$[\mathbf{c}_i^{EE}]_{nm,\nu\mu} = [\mathbf{c}_i^{MM}]_{nm,\nu\mu}. \tag{20d}$$

In the above,

$$\Re g \mathbf{M}_{\nu\mu}(0) = 0,$$

and

$$\Re g \mathbf{N}_{\nu\mu}(0) = 0, \qquad \nu \neq 1,$$

$$\Re g \mathbf{N}_{1,\mp 1}(0) = \frac{2}{3}\sqrt{\frac{3}{8\pi}}(\pm\hat{x} - i\hat{y}),$$

$$\Re g \mathbf{N}_{1,0}(0) = \frac{2}{3}\sqrt{\frac{3}{4\pi}}\hat{z}.$$

Now, assume that the source is located outside V at $\mathbf{r}_s$, $\mathbf{r}_j$ is an interior point, the incident field in the vicinity of $\mathbf{r}_j$ due to source at $\mathbf{r}_s$ can be written as

$$\mathbf{E}^{inc}(\mathbf{r}) = \Re g \overline{\boldsymbol{\psi}}^t(\mathbf{r} - \mathbf{r}_j) \cdot \overline{\boldsymbol{\alpha}}_{js} \cdot \mathbf{a}_s. \tag{21}$$

Applying the equivalence principle, this field can be thought of as coming from the equivalent sources on the boundary:

$$\mathbf{E}^{inc}(\mathbf{r}) = \sum_{i=1}^{N_B} \overline{\boldsymbol{\psi}}^t(\mathbf{r} - \mathbf{r}_i) \cdot \mathbf{b}_i, \tag{22}$$

where $\mathbf{b}_i$ is given by (19c).

Using translation formula to translate $\overline{\boldsymbol{\psi}}^t(\mathbf{r} - \mathbf{r}_i)$, the outgoing wave originated at $\mathbf{r}_i$, to an incoming wave centered at $\mathbf{r}_j$, we have,

$$\overline{\boldsymbol{\psi}}^t(\mathbf{r} - \mathbf{r}_i) = \Re g \overline{\boldsymbol{\psi}}^t(\mathbf{r} - \mathbf{r}_j) \cdot \overline{\boldsymbol{\alpha}}_{ji}. \tag{23}$$

Substituting $\overline{\overline{\psi}}^t(\mathbf{r}-\mathbf{r}_i)$ in (21) by (23), and equating the resultant equation and (22) for arbitrary point $\mathbf{r}$ near $\mathbf{r}_j$, we obtain:

$$\overline{\overline{\alpha}}_{js}\cdot\mathbf{a}_s=\sum_{i=1}^{N_B}\overline{\overline{\alpha}}_{ji}\cdot\overline{\overline{c}}_i\cdot\overline{\overline{\alpha}}_{is}\cdot\mathbf{a}_s=\sum_{i=1}^{N_B}\overline{\overline{h}}_{ji}^{(i)}\cdot\overline{\overline{\alpha}}_{is}\cdot\mathbf{a}_s, \tag{24}$$

with

$$\overline{\overline{h}}_{ji}^{(i)}=\overline{\overline{\alpha}}_{ji}\cdot\overline{\overline{c}}_i. \tag{25}$$

Equation (24) is the second equation which will be used for our equivalence problem.

With Equations (17) and (24), we can easily relate the equivalent interaction matrices $\overline{\overline{I}}_{ij(N_B)}$ with the original ones $\overline{\overline{I}}_{ij(N_A)}$. To this end, we start with Equation (6). We replace $\overline{\overline{\psi}}^t(\mathbf{r}-\mathbf{r}_i)$ of Equation (6) by Equation (17), and replace $\overline{\overline{\alpha}}_{is}\cdot\mathbf{a}_s$ by Equation (24), to obtain

$$\mathbf{E}^{sca}(\mathbf{r})=\sum_{m=1}^{N_B}\overline{\overline{\psi}}^t(\mathbf{r}-\mathbf{r}_m)\cdot\sum_{i=1}^{N_A}\overline{\overline{h}}_{mi}^{(o)}\cdot\sum_{j=1}^{N_A}\overline{\overline{I}}_{ij(N_A)}\cdot\sum_{m'=1}^{N_B}\overline{\overline{h}}_{jm'}^{(i)}\cdot\overline{\overline{\alpha}}_{m's}\cdot\mathbf{a}_s. \tag{26}$$

The above can be rewritten as

$$\mathbf{E}^{sca}(\mathbf{r})=\sum_{m=1}^{N_B}\overline{\overline{\psi}}^t(\mathbf{r}-\mathbf{r}_m)\cdot\sum_{m'=1}^{N_B}\overline{\overline{I}}_{mm'(N_B)}\cdot\overline{\overline{\alpha}}_{m's}\cdot\mathbf{a}_s, \tag{27}$$

where

$$\overline{\overline{I}}_{mm'(N_B)}=\sum_{i=1}^{N_A}\overline{\overline{h}}_{mi}^{(o)}\cdot\sum_{j=1}^{N_A}\overline{\overline{I}}_{ij(N_A)}\cdot\overline{\overline{h}}_{jm'}^{(i)}. \tag{28}$$

Equation (28) specifies the equivalence relation between the original interaction matrices and the equivalent ones. This is the key equation for NEPAL. We will explain how this equation is used to reduce the number of interaction matrices.

For a volume scatterer, the total subscatterers are divided into boundary subscatterers and interior subscatterers. If we define $\overline{\overline{h}}_{mi}^{(o)}=\overline{\overline{h}}_{mi}^{(i)}=\overline{\overline{I}}$ for $i=m$, then the right hand side of equation (28) may also include interaction matrices of boundary subscatterers. Let N_A be the total number of subscatterers, N_B is the number of boundary subscatterers. Then the number of interaction matrices is reduced from N_A^2 to N_B^2 since $N_B<N_A$. Furthermore, there is no violation of addition theorem in using this equivalence principle.

4. The Nested Equivalence Principle Algorithm (NEPAL)

As mentioned in the introduction of this paper, the idea of NEPAL is to reduce the number of scattering centers, or the number of interaction matrices, as shown by Equation (28). In this section, we will describe the steps of this algorithm .

To begin, the subscatterers are first divided into different levels of groups in a nested manner, i.e., a group of one level is divided into two subgroups of the next lower level. Each subgroup is again divided into two subsubgroups of one level lower than that of the subgroup, and so on. The process continues until the lowermost level of subgroups which contains 64 subscatterers is reached. In each level, we find the scattering solution for each of the subgroups, and then use Huygens' equivalence principle (Equation (28)) to replace the interior subscatterers of a subgroup by subscatterers on the boundary. For example, in the lowermost level, we first solve for the scattering solution for each subgroup of 64 subscatterers. Then Equation (28) is used to remove the interior subscatterers. In this level, there are only eight interior subscatterers for each subgroup. After this step, each subgroup contains 56 subscatterers with known solution.

Next we go to the next higher level–the second level. In this level, each subgroup contains 112 subscatterers, as it is made up of two subgroups of 56 subscatterers. The solution to the 112 subscatterers together is not known. Hence, we first solve for the scattering solution for each subgroup with 112 subscatterers, and then their interior subscatterers (8 for each subgroup in this level) are removed via Equation (28) and 104 subscatterers remain in each subgroup with known solution.

We can see that at each level, upon removal of the interior subscatterers, a subgroup contains less subscatterers than what it originally contained. The process is continued until the highest level is reached, where there is only one group which is made up of two lower level subgroups. Again, the solution must be sought for the group. However, since interior subscatterers for the two subgroups are removed, this group contains much less subscatterers than N_A if N_A is the total number of subscatterers for the problem. As a result, much less operations are required to find the solution.

It is seen that the operation at each level contains two parts, one part is to find the scattering solution, the other part is to remove the interior subscatterers. It is important that the removal of the interior subscatterers of a group does not change the scattering property of the subgroup. The solution of interaction matrix can be found in the same way as described in [1].

Using similar analysis as presented for the 2D case, the computational

complexity can be shown to be CN^2 for N spheres, where C is roughly 900.

5. Parallelization of the Code on CM-5

There are two major processes in implementing NEPAL: they are the interaction matrix algorithm (IMA) process and the equivalence principle process. The IMA consumes most of the CPU time. When NEPAL was first implemented on the Thinking Machine Corp., CM-5, the code calls an external function in the library of CM-5. This function inverts a matrix by Gauss-Jordan method (the name of the function is "gen_gj_invert"). When this function is called in the IMA part, we found that the CPU time for matrix fill is dominant, because the matrix inverse is greatly expedited. This was not the case on a serial machine. Hence, we seek to expedite the matrix fill as follows.

The matrix involved in the IMA can be written as

$$\overline{\mathbf{A}} = [\overline{\mathbf{A}}_{ij}]$$

where $\overline{\mathbf{A}}_{ij}$ are block matrices.

$$\overline{\mathbf{A}}_{ij} = \begin{cases} \bar{\mathbf{I}}, & i = j, \\ -\overline{\mathbf{T}}_{k(1)} \cdot \overline{\boldsymbol{\alpha}}_{ij}, & i \pm j, \end{cases}$$

and $\overline{\mathbf{T}}_{i(1)}$ are the isolated T-matrix. $\overline{\boldsymbol{\alpha}}_{ij}$ are the wave translation matrices[2]. For this specific problem, the size of the subscatterrer is small compared to wavelength. As a result, the size of the translation matrices is 6×6, as it can be given explicitly as:

$$\overline{\mathbf{A}}_{ij} = \begin{bmatrix} \overline{\boldsymbol{\alpha}} & \overline{\boldsymbol{\beta}} \\ \overline{\boldsymbol{\beta}} & \overline{\boldsymbol{\alpha}} \end{bmatrix}$$

where

$$[\overline{\boldsymbol{\alpha}}_{ij}]_{12} = \frac{3}{2\sqrt{2}} h_2 \sin\theta_{ij} \cos\theta_{ij} e^{i\phi_{ij}}$$

$$[\overline{\boldsymbol{\alpha}}_{ij}]_{22} = h_0 + h_2(1.5\cos^2\theta_{ij} - \frac{1}{2})$$

$$[\overline{\boldsymbol{\alpha}}_{ij}]_{13} = -0.75\sin^2\theta_{ij} h_2 e^{i2\phi_{ij}}$$

$$[\overline{\boldsymbol{\alpha}}_{ij}]_{33} = h_0 - \frac{1}{2}([\alpha_{ij}]_{22} - h_0)$$

$$[\overline{\boldsymbol{\beta}}_{ij}]_{12} = \frac{3i}{2\sqrt{2}} h_1 \sin\theta_{ij} e^{i\phi_{ij}}$$

$$
\begin{aligned}
[\overline{\beta}_{ij}]_{33} &= \frac{3}{2} i h_1 \cos\theta_{ij} \\
[\overline{\alpha}_{ij}]_{11} &= [\overline{\alpha}_{ij}]_{33} \\
[\overline{\alpha}_{ij}]_{21} &= [\overline{\alpha}_{ij}]_{12} e^{-i2\phi_{ij}} \\
[\overline{\alpha}_{ij}]_{23} &= -[\overline{\alpha}_{ij}]_{12} \\
[\overline{\alpha}_{ij}]_{31} &= [\overline{\alpha}_{ij}]_{13} e^{-i4\phi_{ij}} \\
[\overline{\alpha}_{ij}]_{32} &= -[\overline{\alpha}_{ij}]_{12} \\
[\overline{\beta}_{ij}]_{11} &= -[\overline{\beta}_{ij}]_{33} \\
[\overline{\beta}_{ij}]_{21} &= [\overline{\beta}_{ij}]_{12} e^{-i\phi_{ij}} \\
[\overline{\beta}_{ij}]_{23} &= [\overline{\beta}_{ij}]_{12} \\
[\overline{\beta}_{ij}]_{32} &= [\overline{\beta}_{ij}]_{21} \\
[\overline{\beta}_{ij}]_{13} &= -[\overline{\beta}_{ij}]_{22} = [\overline{\beta}_{ij}]_{31} = 0.
\end{aligned}
$$

In the above, h_0, h_1, and h_2 are the spherical Hankel functions with the appropriate arguments. With this explicit expression, it is easy to parallelize the matrix-fill part. We know that one of the strength of CM-5 is on matrix operations. Hence, instead of using "do loops" in standard FORTRAN to compute r_{ij}, θ_{ij}, ϕ_{ij}, and $h_0(kr_{ij})$, etc., for each $i, j = 1, 2, \ldots, N$, we use the statement on the CM-5,

```
for all (i=1:n, j=1:n) r(i,j)=sqrt((x(i)-x(j))**2
                                  +(y(i)-y(j))**2
                                  +(z(i)-z(j))**2)
```

to compute r_{ij}, and similarly for θ_{ij}, ϕ_{ij}. Having obtained the above, we can compute the following efficiently by performing matrix operations. For example, the CM-5 FORTRAN code will appear as

```
h_0=exp(i*k_0*r)/(k_0*r)
h_1=h_0*(1/(k_0*r)-1)
h_2=3*h_1/(k_0*r)-h_0
beta(:,:,3,3)=1.5*i*cos(theta)*h_1
```

This paprallel implementation makes the matrix-fill part a small portion of total CPU time. A similar proceduce is used to parallelize the computation of $\overline{\mathbf{h}}^{(i)}$ and $\overline{\mathbf{h}}^{(o)}$ matrices.

We estimate a throughput of about 1 GFLOPS on a 64 processor partition of the CM-5.

6. Numerical Results

Using this algorithm, we have developed a program to compute the scattering solution of rectangular cubic dielectric scatterers. In our numerical simulation, 6 spherical modes (3 for TE and 3 for TM) are used to expand the scattered field of a subscatterer. Figure 2 and Figure 3 show the scattered field (magnitude and phase, respectively) of a cubic dielectric scatterer with side length $a = b = c = 1.6\lambda$ and $\epsilon_r = 2.6$. The incident wave is coming from $\theta = 180^0$ and $\phi = 0^0$ with θ polarization and frequency of 300 MHz. The scattered field is observed at $\theta = 0^0$ to $\theta = 180^0$ and $\phi = 0^0$. Only the E_θ component is ploted. The results agree well with that of the brute force solution using Gaussian elimination.

In Figure 4, we compute the RCS of a low observable target which is a foamy cylinder of diameter 1.2 λ_0, and length 2.1 λ_0, with $\epsilon_r = 1.05 + i0.2$. It took about 2,000 s of CPU on a 128 processor partition of the CM-5, and 2.66 GB of memory. The result compares reasonably well with a brute force method. The brute force method uses a Neumann type iteration, and converges quite quickly because of the low contrast of the scatterer. For the computation of 31 points using 9 iterations, it took about 600 s of CPU on the CM-5 with 329 MB of memory.

As for the computational complexity, Figure 5 shows the comparison of the CPU time (on CM-5) of this method (NEPAL) with the brute force solution using LU decomposition. It is seen that when N, the number of unknowns, is small, NEPAL is not as efficient as brute force. However, when N is large, NEPAL uses less CPU time than brute force. The cross over occurs at about $N = 1800$. It is also seen that the slope of the CPU time curve for NEPAL is decreasing, and approaches the slope of an N^2 curve.

7. Conclusion

We have presented in this paper the extension of the nested equivalence principle algorithm (NEPAL) to three dimensions. The algorithm is based on Huygens' equivalence principle and nesting small algorithms within a larger one. Therefore, the key element is to divide the computation into several stages and reduce the number of unknowns at each stage. This represents an efficient algorithm for directly solving the integral equation of scattering with reduced computational complexity of $O(N^2)$. Hence, it can be used to compute the scattering solution of large objects for many incident waves.

References

[1] W. C. Chew and C. C. Lu, "The use of Huygens' equivalence principle for solving the volume integral equation of scattering," *IEEE Trans.*

Antennas Propagat., vol. AP-41, no. 7, pp. 897-904, July 1993.

[2] Y. M. Wang and W. C. Chew, "A recursive T-matrix approach for the solution of electromagnetic scattering by many spheres," *IEEE Trans. Antennas Propagat.*, vol. AP-41, no. 12, pp. 1633-1639, December 1993.

[3] W. C. Chew, *Waves and Fields in Inhomogeneous Media*: Van Nostrand Reinhold, New York, 1990.

[4] J. D. Jackson, *Classical Electrodynamics* , Second Edition, John Wiley & Sons, New York, 1975.

[5] W. C. Chew and Y. M. Wang, " Efficient ways to compute the vector addition theorem," *J. Electromag. Waves and Appl.*, vol.7, no. 5, pp.651-665, 1993.

[6] W. C. Chew, J. Friedrich, and R. Geiger, "A multiple scattering solution for the effective permittivity of a sphere mixture," *IEEE Geoscience and Remote Sensing*, vol. 28, no. 2, p. 207, 1990.

[7] B. Peterson and S. Ström, "T-matrix for electromagnetic scattering from an arbitray number of scatterers and representation of E(3)," *Phys. Rev.*, D8, pp. 3661-3678, 1973.

[8] C. Lanczos, *Applied Analysis*, p.41, Prentice-Hall, Englewood Cliffs, N. J. 1956.

[9] L. Gurel and W. C. Chew, "Recursive algorithms for calculating the scattering from N strips or patches," *IEEE Trans. Antennas Propagat.*, vol. AP-38, no. 4, pp. 507-515, April 1990.

[10] A. George, "Nested dissection of a regular finite element mesh," *SIAM J. Numer. Anal.*, vol. 10, pp. 345-363, 1973.

[11] W. H. Weedon and W. C. Chew, "Time-domain inverse scattering using the local shape function (LSF) method," *Incerse Problems*, vol. 9, pp. 551-564, 1993.

[12] L. Tsang and C. E. Mandt, "Monte-carlo simulations of the extinction rate of dense media with randomly distributed dielectric spheres based on solution of Maxwell's equations," *Optics Letters*, vol. 17, No. 5, pp. 314-316, March 1, 1992.

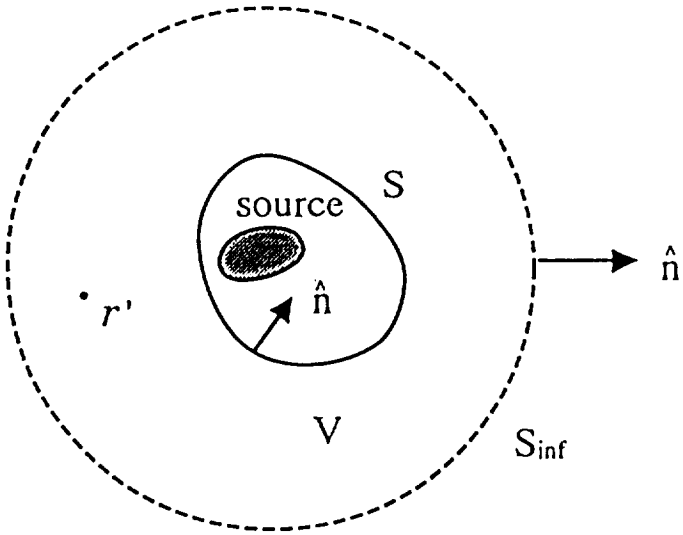

Figure 1. The Huygens' equivalence principle.

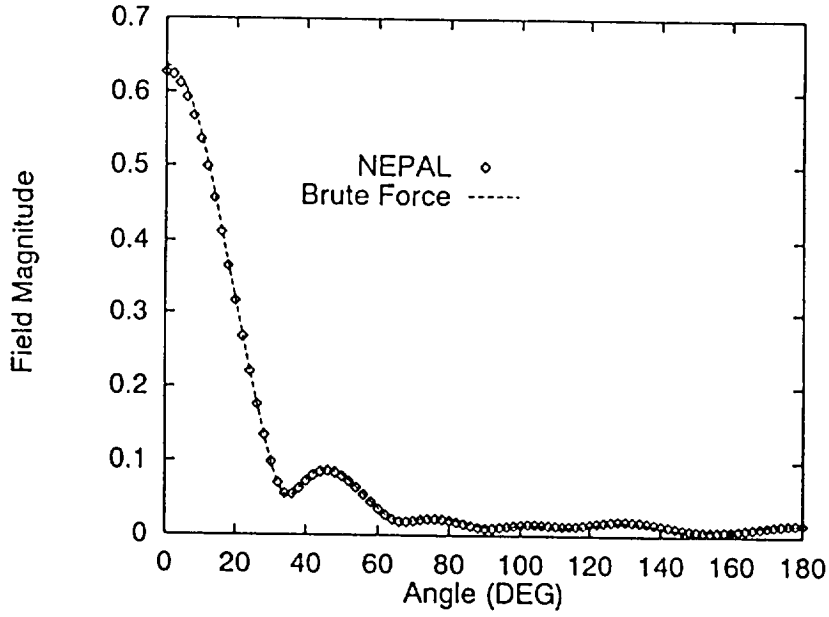

Figure 2. Scattered field (magnitude) of a cubic dielectric scatterer for plane wave incidence at $\theta = 180°$. Side length $= 1.6\lambda$, $\epsilon_r = 2.6$, $f = 300(MHz)$. Field points are on the circle of $r = 10\lambda$. The cubic is divided into 512 small subscatterers.

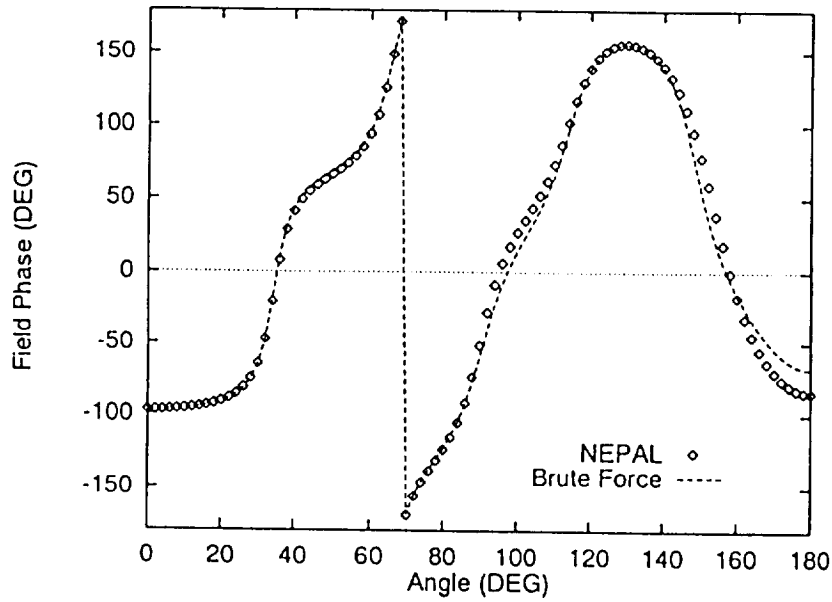

Figure 3. Scattered field (phase) of a dielectric cubic with the same parameters as in Figure 3.

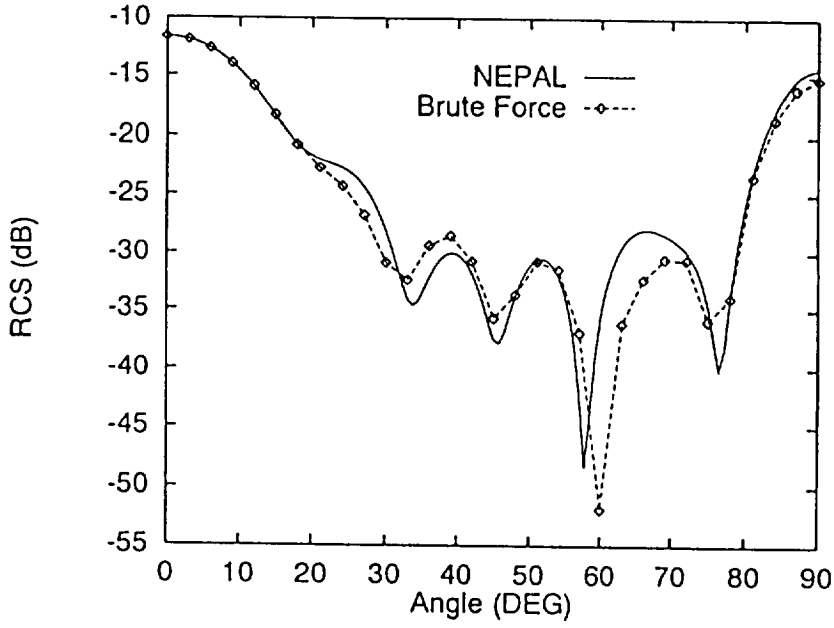

Figure 4. Comparison of the RCS of a low-observable target with a brute-force iterative approach.

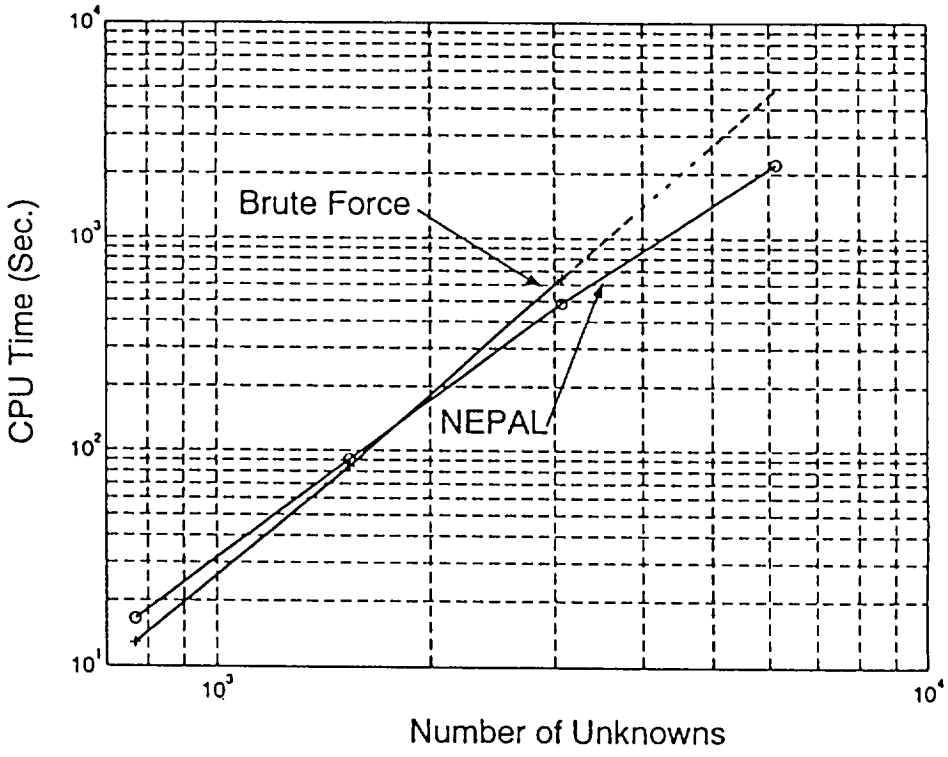

Figure 5. Comparison of CPU time of NEPAL and Gaussian elimination.

CHAPTER 2

PARALLELIZATION OF FDTD CODE ON CM-5 USING PML MATERIAL ABSORBING BOUNDARY CONDITION

1. Introduction

The finite difference time domain method [1,2] is widely regarded as one of the most popular computational electromagnetics algorithms. Although FDTD is conceptually very simple and relatively easy to program, the method is actually quite efficient since it involves $O(N^{1.5})$ computational complexity in 2-D and $O(N^{1.33})$ computational complexity in 3-D [3]. In fact, FDTD can be considered an optimal algorithm since $O(N^{\alpha})$ numbers are produced in $O(N^{\alpha})$ operations.

FDTD is also ideally suited for implementation on a single-instruction multiple-data (SIMD) massively parallel computer. The reason is that the stencil operations that must be computed at each node of the space grid involve only nearest-neighbor interactions and may be implemented at a minimum communication cost [4]. A major challenge, however, is in implementing absorbing boundary conditions (ABCs) at the edges of the FDTD grid. On scalar and vector computers, these boundary conditions are typically computed using methods such as the Engquist-Majda [5], Mur [6], Liao [7] or Higdon [8] ABC. However, these methods are not ideal for parallel supercomputers since they all involve communication with many elements normal to the grid boundary. Such communication can easily surpass the time spent computing core FDTD operations in the grid interior, especially for higher-order boundary conditions, and hence can become a bottleneck in the FDTD code. Also, they do not allow for SIMD operation on a parallel machine without the use of masking.

An alternate method of implementing an ABC is to use a conventional absorbing material boundary [4, 9–14]. For SIMD parallel computation, these methods have the advantage that the ABC may be implemented with the same FDTD stencil operation as the interior nodes by modifying the conductivity material parameter at the edge of the FDTD grid. The disadvantage is that the reflection coefficient at the absorbing border is zero only at normal incidence and is both angle and frequency dependent. Consequently, the ab-

sorbing material border region must be made quite large—typically 20–100 grid points along each edge in order to minimize reflections.

Recently, Berenger [15] suggested a more general method of implementing an absorbing material boundary condition. Berenger proposed a procedure for 2-D wave propagation whereby Maxwell's equations are generalized and added degrees of freedom are introduced. The added degrees of freedom allow the specification of absorbing borders with zero reflection coefficient at all angles of incidence and all frequencies. Moreover, the generalized Maxwell's equations reduce to the familiar Maxwell's equations as a special case and hence the same generalized equations can be used to propagate fields in both the interior region and absorbing region. Although the interface between the interior region and the absorbing boundary is reflectionless, there is still a reflection from the edge of the grid. The advantage of using Berenger's procedure is that much larger conductivity values may be specified in the absorbing region, leading to a drastic reduction in the number of grid points required for the absorbing boundary.

In the present paper, a formulation similar to the Berenger idea is derived for 3-D wave propagation from first principles using a coordinate stretching approach. The advantage of the new method for SIMD parallel computation is stressed. The method is validated with 3-D FDTD numerical computations on a Thinking Machines Corporation Connection Machine CM-5.

2. Modified Maxwell's Equations

For a general medium, we define the modified Maxwell's equations in the frequency domain, assuming $e^{-i\omega t}$ time dependence, as

$$\nabla_e \times \mathbf{E} = i\omega\mu\mathbf{H} \tag{1}$$

$$\nabla_h \times \mathbf{H} = -i\omega\epsilon\mathbf{E} \tag{2}$$

$$\nabla_h \cdot \epsilon\mathbf{E} = \rho \tag{3}$$

$$\nabla_e \cdot \mu\mathbf{H} = 0 \tag{4}$$

where

$$\nabla_e = \hat{x}\frac{1}{e_x}\frac{\partial}{\partial x} + \hat{y}\frac{1}{e_y}\frac{\partial}{\partial y} + \hat{z}\frac{1}{e_z}\frac{\partial}{\partial z} \tag{5}$$

$$\nabla_h = \hat{x}\frac{1}{h_x}\frac{\partial}{\partial x} + \hat{y}\frac{1}{h_y}\frac{\partial}{\partial y} + \hat{z}\frac{1}{h_z}\frac{\partial}{\partial z}. \tag{6}$$

In the above, e_i, h_i, $i = x, y, z$ are coordinate-stretching variables that stretch the x, y, z coordinates for ∇_e and ∇_h. It shall be shown later that when e_i and h_i are complex numbers, the medium can be lossy. Note that (3) and (4) are derivable from (1) and (2). A general plane wave solution to Equations (1) – (4) has the form

$$\mathbf{E} = \mathbf{E}_0 \, e^{i\mathbf{k}\cdot\mathbf{r}} \tag{7}$$

and

$$\mathbf{H} = \mathbf{H}_0 \, e^{i\mathbf{k}\cdot\mathbf{r}} \tag{8}$$

where $\mathbf{k} = \hat{x}k_x + \hat{y}k_y + \hat{z}k_z$. Substituting Equations (7) and (8) into Equations (1) and (2) above gives

$$\mathbf{k}_e \times \mathbf{E} = \omega\mu\mathbf{H} \tag{9}$$

$$\mathbf{k}_h \times \mathbf{H} = -\omega\epsilon\mathbf{E}, \tag{10}$$

where $\mathbf{k}_e = \hat{x}\frac{k_x}{e_x} + \hat{y}\frac{k_y}{e_y} + \hat{z}\frac{k_z}{e_z}$ and $\mathbf{k}_h = \hat{x}\frac{k_x}{h_x} + \hat{y}\frac{k_y}{h_y} + \hat{z}\frac{k_z}{h_z}$. Combining the above, we have

$$\begin{aligned} -\omega^2\mu\epsilon\mathbf{H} &= \mathbf{k}_e \times \mathbf{k}_h \times \mathbf{H} \\ &= \mathbf{k}_h(\mathbf{k}_e \cdot \mathbf{H}) - (\mathbf{k}_e \cdot \mathbf{k}_h)\mathbf{H}. \end{aligned} \tag{11}$$

But from Equation (9), $\mathbf{k}_e \cdot \mathbf{H} = 0$ for a homogeneous medium. This gives the dispersion relation

$$\omega^2\mu\epsilon = \mathbf{k}_e \cdot \mathbf{k}_h \tag{12}$$

or

$$\kappa^2 = \frac{1}{e_x h_x}k_x^2 + \frac{1}{e_y h_y}k_y^2 + \frac{1}{e_z h_z}k_z^2 \tag{13}$$

where $\kappa^2 = \omega^2\mu\epsilon$. Equation (13) is the equation of an ellipsoid in 3-D and is satisfied by

$$k_x = \kappa\sqrt{e_x h_x}\sin\theta\cos\phi, \tag{14}$$

$$k_y = \kappa\sqrt{e_y h_y}\sin\theta\sin\phi, \tag{15}$$

and

$$k_z = \kappa\sqrt{e_z h_z}\cos\theta. \tag{16}$$

Note that when e_i, h_i, $i = x, y, z$ are complex, the wave in the x, y, and z directions are attenuative and can be independently controlled. Under the

matching condition, $e_x = h_x$, $e_y = h_y$, and $e_z = h_z$, we have $|\mathbf{k}_e|^2 = |\mathbf{k}_h|^2 = \kappa^2$. The wave impedance is then given by

$$\eta = \frac{|\mathbf{E}|}{|\mathbf{H}|} = \frac{|\mathbf{k}_h|}{\omega\epsilon} = \sqrt{\frac{\mu}{\epsilon}}, \tag{17}$$

irrespective of the values for $e_i, i = x, y, z$ and the direction of propagation.

3. Single Interface Problem

Assume that a plane wave is obliquely incident on the interface $z = 0$ in Figure 1. Furthermore, we may assume that the plane wave is of arbitrary polarization. The incident field may be decomposed into a sum of two components, one with electric field transverse to z (TE^z) and the other with magnetic field transverse to z (TM^z). We will examine these two components individually.

In the (TE^z) case, we let the incident field in region 1 be given as

$$\mathbf{E}_i = \mathbf{E}_0\, e^{i\mathbf{k}_i\cdot\mathbf{r}}. \tag{18}$$

In the above, $\mathbf{k}_{hi} \cdot \mathbf{E}_0 = 0$, and $\mathbf{E}_0$ is in the xy plane. Similarly, we define the reflected field in region 1 as

$$\mathbf{E}_r = R^{\mathrm{TE}}\, \mathbf{E}_{0r}\, e^{i\mathbf{k}_r\cdot\mathbf{r}} \tag{19}$$

and the transmitted field in region 2 as

$$\mathbf{E}_t = T^{\mathrm{TE}}\, \mathbf{E}_{0t}\, e^{i\mathbf{k}_t\cdot\mathbf{r}}. \tag{20}$$

Phase matching requires that $k_{ix} = k_{rx} = k_{tx}$ and $k_{iy} = k_{ry} = k_{ty}$. Hence, we can define $\mathbf{E}_{0r} = \mathbf{E}_{0t} = \mathbf{E}_0$ since they all point in the same direction. Applying the boundary condition that the tangential electric field must be continuous across the plane $z = 0$,* we have

$$1 + R^{\mathrm{TE}} = T^{\mathrm{TE}}. \tag{21}$$

The magnetic field may be determined using Equation (9) for regions 1 and 2 as

$$\mathbf{H}_1 = \frac{\mathbf{k}_{ie} \times \mathbf{E}_0}{\omega\mu_1}\, e^{i\mathbf{k}_i\cdot\mathbf{r}} + R^{\mathrm{TE}}\, \frac{\mathbf{k}_{re} \times \mathbf{E}_0}{\omega\mu_1}\, e^{i\mathbf{k}_r\cdot\mathbf{r}} \tag{22}$$

* This boundary condition follows from the modified Maxwell's equation (1).

and

$$\mathbf{H}_2 = T^{\mathrm{TE}} \frac{\mathbf{k}_{te} \times \mathbf{E}_0}{\omega \mu_2} e^{i\mathbf{k}_t \cdot \mathbf{r}} \tag{23}$$

where $\mathbf{k}_{ie} = \hat{x}\frac{k_{ix}}{e_x} + \hat{y}\frac{k_{iy}}{e_y} + \hat{z}\frac{k_{iz}}{e_z}$ and similarly for $\mathbf{k}_{re}$ and $\mathbf{k}_{te}$. We also define $k_{1z} = k_{iz}$, $k_{2z} = k_{tz}$ and note that $k_{rz} = -k_{1z}$. Then equating the tangential components of Equations (22) and (23), we have

$$k_{1z} e_{2z} \mu_2 \left[1 - R^{\mathrm{TE}}\right] = T^{\mathrm{TE}} k_{2z} e_{1z} \mu_1. \tag{24}$$

Combining Equations (21) and (24), we have

$$R^{\mathrm{TE}} = \frac{k_{1z} e_{2z} \mu_2 - k_{2z} e_{1z} \mu_1}{k_{1z} e_{2z} \mu_2 + k_{2z} e_{1z} \mu_1} \tag{25}$$

and

$$T^{\mathrm{TE}} = \frac{2 k_{1z} e_{2z} \mu_2}{k_{1z} e_{2z} \mu_2 + k_{2z} e_{1z} \mu_1}. \tag{26}$$

Applying a similar procedure to the TM^z component, we have

$$R^{\mathrm{TM}} = \frac{k_{1z} h_{2z} \epsilon_2 - k_{2z} h_{1z} \epsilon_1}{k_{1z} h_{2z} \epsilon_2 + k_{2z} h_{1z} \epsilon_1} \tag{27}$$

and

$$T^{\mathrm{TM}} = \frac{2 k_{1z} h_{2z} \epsilon_2}{k_{1z} h_{2z} \epsilon_2 + k_{2z} h_{1z} \epsilon_1}. \tag{28}$$

4. A Perfectly Matched Interface

The phase matching condition requires that $k_{1x} = k_{2x}$ and $k_{1y} = k_{2y}$, or

$$\kappa_1 \sqrt{e_{1x} h_{1x}} \sin\theta_1 \cos\phi_1 = \kappa_2 \sqrt{e_{2x} h_{2x}} \sin\theta_2 \cos\phi_2 \tag{29}$$

and

$$\kappa_1 \sqrt{e_{1y} h_{1y}} \sin\theta_1 \sin\phi_1 = \kappa_2 \sqrt{e_{2y} h_{2y}} \sin\theta_2 \sin\phi_2 \tag{30}$$

where $\kappa_1 = \omega\sqrt{\mu_1 \epsilon_1}$ and $\kappa_2 = \omega\sqrt{\mu_2 \epsilon_2}$. For a perfectly matched medium, we choose $\epsilon_1 = \epsilon_2$, $\mu_1 = \mu_2$, $e_x = h_x$ and $e_y = h_y$. Equations (29) and (30) become

$$e_{1x} \sin\theta_1 \cos\phi_1 = e_{2x} \sin\theta_2 \cos\phi_2 \tag{31}$$

and

$$e_{1y} \sin\theta_1 \sin\phi_1 = e_{2y} \sin\theta_2 \sin\phi_2. \tag{32}$$

If we now choose $e_{1x} = e_{2x}$ and $e_{1y} = e_{2y}$, then $\theta_1 = \theta_2$, $\phi_1 = \phi_2$ and we can show that both $R^{\mathrm{TE}} = 0$ and $R^{\mathrm{TM}} = 0$ for all angles of incidence and all frequencies.

If region 1 is a vacuum, then $\mu = \mu_0$, $\epsilon = \epsilon_0$, and

$$(e_{1x}, e_{1y}, e_{1z}, h_{1x}, h_{1y}, h_{1z}) = (1, 1, 1, 1, 1, 1). \tag{33}$$

In order to have a lossy region 2 with no reflections at the region 1/region 2 interface, we choose

$$(e_{2x}, e_{2y}, e_{2z}, h_{2x}, h_{2y}, h_{2z}) = (1, 1, s_2, 1, 1, s_2) \tag{34}$$

where s_2 is a complex number. In this case,

$$k_{1x} = k_{2x} = \kappa_0 \sin\theta \cos\phi \tag{35}$$

$$k_{1y} = k_{2y} = \kappa_0 \sin\theta \sin\phi \tag{36}$$

$$k_{1z} = \kappa_0 \cos\theta \tag{37}$$

$$k_{2z} = \kappa_0 s_2 \cos\theta \tag{38}$$

where $\kappa_0 = \omega\sqrt{\mu_0\epsilon_0}$. If $s_2 = s_2' + is_2''$, the wave will attenuate in the z direction. This kind of interface is useful for building material ABCs in a FDTD simulation.

5. Modified Equations in the Time Domain

For the general case of a matched medium, we let $e_x = h_x = s_x$, $e_y = h_y = s_y$ and $e_z = h_z = s_z$. Then, $\nabla_e = \nabla_h = \hat{x}\frac{1}{s_x}\frac{\partial}{\partial x} + \hat{y}\frac{1}{s_y}\frac{\partial}{\partial y} + \hat{z}\frac{1}{s_z}\frac{\partial}{\partial z}$. In Equation (1), we write the curl as

$$\nabla_e \times \mathbf{E} = \frac{1}{s_x}\frac{\partial}{\partial x}\hat{x} \times \mathbf{E} + \frac{1}{s_y}\frac{\partial}{\partial y}\hat{y} \times \mathbf{E} + \frac{1}{s_z}\frac{\partial}{\partial z}\hat{z} \times \mathbf{E}. \tag{39}$$

Then, defining $\mathbf{H}_{s_x}$, $\mathbf{H}_{s_y}$, and $\mathbf{H}_{s_z}$ in terms of the components of Equation (39), we let

$$i\omega\mu\mathbf{H}_{s_x} = \frac{1}{s_x}\frac{\partial}{\partial x}\hat{x} \times \mathbf{E} \tag{40}$$

$$i\omega\mu\mathbf{H}_{s_y} = \frac{1}{s_y}\frac{\partial}{\partial y}\hat{y} \times \mathbf{E} \tag{41}$$

and

$$i\omega\mu\mathbf{H}_{s_z} = \frac{1}{s_z}\frac{\partial}{\partial z}\hat{z} \times \mathbf{E} \tag{42}$$

where $\mathbf{H} = \mathbf{H}_{s_x} + \mathbf{H}_{s_y} + \mathbf{H}_{s_z}$. Similarly, we can write Equation (2) as

$$-i\omega\epsilon\mathbf{E}_{s_x} = \frac{1}{s_x}\frac{\partial}{\partial x}\hat{x} \times \mathbf{H} \tag{43}$$

$$-i\omega\epsilon\mathbf{E}_{s_y} = \frac{1}{s_y}\frac{\partial}{\partial y}\hat{y} \times \mathbf{H} \tag{44}$$

and

$$-i\omega\epsilon\mathbf{E}_{s_z} = \frac{1}{s_z}\frac{\partial}{\partial z}\hat{z} \times \mathbf{H}. \tag{45}$$

where $\mathbf{E} = \mathbf{E}_{s_x} + \mathbf{E}_{s_y} + \mathbf{E}_{s_z}$. Note that $\mathbf{H}_{s_i}$, $\mathbf{E}_{s_i}$, $i = x, y, z$ are two-component vectors.

We now let $s_x = 1 + i\sigma_x/\omega\epsilon$, $s_y = 1 + i\sigma_y/\omega\epsilon$ and $s_z = 1 + i\sigma_z/\omega\epsilon$. Writing Equations (40) - (42) and (43) - (45) in the time domain, we have

$$\mu\frac{\partial\mathbf{H}_{s_x}}{\partial t} + \frac{\sigma_x\mu}{\epsilon}\mathbf{H}_{s_x} = -\frac{\partial}{\partial x}\hat{x} \times \mathbf{E} \tag{46}$$

$$\mu\frac{\partial\mathbf{H}_{s_y}}{\partial t} + \frac{\sigma_y\mu}{\epsilon}\mathbf{H}_{s_y} = -\frac{\partial}{\partial y}\hat{y} \times \mathbf{E} \tag{47}$$

$$\mu\frac{\partial\mathbf{H}_{s_z}}{\partial t} + \frac{\sigma_z\mu}{\epsilon}\mathbf{H}_{s_z} = -\frac{\partial}{\partial z}\hat{z} \times \mathbf{E} \tag{48}$$

and

$$\epsilon\frac{\partial\mathbf{E}_{s_x}}{\partial t} + \sigma_x\mathbf{E}_{s_x} = \frac{\partial}{\partial x}\hat{x} \times \mathbf{H} \tag{49}$$

$$\epsilon\frac{\partial\mathbf{E}_{s_y}}{\partial t} + \sigma_y\mathbf{E}_{s_y} = \frac{\partial}{\partial y}\hat{y} \times \mathbf{H} \tag{50}$$

$$\epsilon\frac{\partial\mathbf{E}_{s_z}}{\partial t} + \sigma_z\mathbf{E}_{s_z} = \frac{\partial}{\partial z}\hat{z} \times \mathbf{H}. \tag{51}$$

Equations (46) - (51) described 3-D wave propagation in a perfectly matched medium. The wave propagation phenomenon described by these equations is very similar to that described by Maxwell's equations with the exception that attenuation may be controlled through the σ_x, σ_y and σ_z variables. The FDTD implementation of these equations on a Yee FDTD grid is

straightforward. Absorbing boundaries at the edges of the simulation region may be created by choosing appropriate values of σ_x, σ_y and σ_z. Equations (46) - (51) may be seen to include Berenger's equations [berenger1] as a subset for the 2-D TE or TM case.

The above equations involve 12 components of electromagnetic fields. For a free-space/lossy medium interface, a scheme may be devised using only 10 field components for the 3-D case, and only 3 components for the 2-D case. However, this is achieved at the loss of SIMD operation on a parallel machine.

6. Computer Simulation Results

In order to demonstrate the new method, a 3-D orthogonal grid FDTD algorithm was developed based on Equations (46) - (51). The FDTD algorithm was implemented as a SIMD code on the Thinking Machines Corporation Connection Machine CM-5. The algorithm operates very efficiently on the CM-5 because the FDTD stencil operations that need to be computed at each node involve only nearest-neighbor interactions. The communication operations resulting from the nearest-neighbor interactions are at a minimum cost since the neighboring processors are for the most part at the bottom of the fat-tree communication network, where communication bandwidth is maximum.

To validate our 3-D FDTD algorithm, we solved a simple problem of computing the field radiated from an infinitesimal electric dipole in free space. An analytic solution was also computed in the frequency domain for many excitation frequencies. The frequency domain solution was then multiplied by the spectrum of FDTD source pulse and inverse Fourier transformed to yield a time-domain analytic solution for comparison with the FDTD solution.

The FDTD solution was solved in a cubic region of dimension

$$(N_x, N_y, N_z) = (128, 128, 32)$$

grid points. The grid parameters chosen were $\Delta x = \Delta y = \Delta z = 2.5\text{mm}$, $\Delta t = 4.5\text{ps}$ and $N_t = 512$ time steps were computed.

The infinitesimal electric dipole was simulated by exciting the E_y field in a single grid cell with the source pulse

$$J_y(t) = \frac{1}{\Delta x \Delta y \Delta z} \left[4(t/\tau)^3 - (t/\tau)^4\right] e^{-t/\tau} \tag{52}$$

where $\tau = 1/4\pi f_0$ and a value of $f_0 = 1.0\text{GHz}$ was chosen. The dipole source was located at grid location $(n_x, n_y, n_z) = (91, 64, 16)$. The E_x and E_y fields were obtained by sampling the fields at grid location $(n_x, n_y, n_z) = (37, 91, 16)$.

The absorbing boundaries used for the FDTD simulation consisted of planar layers of thickness 8 grid points on all surfaces. Along the borders parallel to x axis, the value of σ_x was specified, while σ_y and σ_z were specified on the borders parallel to the y and z axis, respectively. The conductivity values were chosen with a parabolic taper decreasing from the maximum value towards the center of the grid such that the reflection coefficient at normal incidence was $R_0 = .0001$.

The E_x field computed using both the analytic formulation and the FDTD algorithm are overlaid in Figure 2. The curves due to the analytic and numerical solutions are barely distinguishable, indicating excellent agreement. Similarly, the E_y field due to the analytic and numerical solutions are overlaid in Figure 3. Again, we see excellent agreement. Any difference between the analytic and numerical solutions in Figures 2 and 3 may be attributed to modeling errors such as the finite size of the dipole source and the discrete approximation of Maxwell's equations in addition to reflections due to imperfections in the absorbing boundaries.

The CM-5 machine used to solve the FDTD problem is located at the National Center for Supercomputing Applications (NCSA) at the University of Illinois. The program was written in CM Fortran and compiled using CMF version 2.1. The CM-5 at the NCSA has 512 nodes with vector units. CPU times were determined by running the problem on 32, 64, 128 and 256 node partitions. For this problem, a total of 0.5 million unknown field quantities ($128 \times 128 \times 32$ grid) were determined for 512 time steps. The CPU times are shown in Table 1.

7. Conclusions

A modified set of Maxwell's equations have been introduced using complex coordinate stretching factors along the three cartesian coordinate axis. This modification introduces additional degrees of freedom in Maxwell's equations such that absorbing boundaries may be specified with zero reflection coefficient at all frequencies and all angles of incidence. The formulation was shown to be related to the perfectly matched layer that was recently derived by Berenger for 2-D wave propagation. A 3-D FDTD algorithm was developed from the modified Maxwell's equations that uses the reflectionless absorbing interface property to implement radiation boundary conditions at the edges of the FDTD grid. The accuracy of the algorithm was validated by computing the field radiated from an infinitesimal electric dipole and comparing against a known analytical expression. The FDTD algorithm was implemented on the Connection Machine CM-5 and timing results were presented. This breakthrough in absorbing material boundary conditions allows EM scattering to be computed very efficiently on SIMD parallel computers.

Acknowledgement

The authors wish to thank J. P. Berenger for sending us a preprint of his work and to A. Taflove for bringing to our attention J. P. Berenger's work.

References

[1] K. S. Yee, "Numerical solution of initial boundary value problems involving Maxwell's equations in isotropic media," *IEEE Trans. Antennas Propagat.*, vol. AP-14, pp. 302–307, 1966.

[2] A. Taflove, "Review of the formulation and applications of the finite-difference time-domain method for numerical modeling of electromagnetic wave interactions with arbitrary structures," *Wave Motion*, vol. 10, pp. 547–582, 1988.

[3] W. C. Chew, *Waves and Fields in Inhomogeneous Media.* New York: Van Nostrand, 1990.

[4] W. H. Weedon, W. C. Chew, and C. M. Rappaport, "Computationally efficient FDTD simulation of open-region scattering problems on the connection machine CM-5," in *IEEE Antennas and Propagation Society International Symposium Digest*, (Seattle, WA), June 19–24, 1994.

[5] B. Engquist and A. Majda, "Absorbing boundary conditions for the numerical simulation of waves," *Math. Computation*, vol. 31, pp. 629–651, 1977.

[6] G. Mur, "Absorbing boundary conditions for the finite-difference approximation of the time-domain electromagnetic field equations," *IEEE Trans. Electromag. Compat.*, vol. EMC-23, pp. 377–382, 1981.

[7] Z. P. Liao, H. L. Wong, B. P. Yang, and Y. F. Yuan, "A transmitting boundary for transient wave analysis," *Scientia Sinica. (Series A)*, vol. 27, no. 10, pp. 1063–1076, 1984.

[8] R. L. Higdon, "Numerical absorbing boundary conditions for the wave equation," *Math. Comput.*, vol. 49, pp. 65–90, 1987.

[9] I. Katz, D. Parks, A. Wilson, M. Rotenberg, and J. Harren, "Non-reflective free space boundary conditions for SGEMP codes," *Systems, Science and Software*, vol. SSS-R-76-2934, 1976.

[10] R. Holland and J. W. Williams, "Total-field versus scattered-field finite-difference codes: A comparative assessment," *IEEE Trans. Nuclear Sci.*, vol. NS-30, pp. 4583–4588, 1983.

[11] J.-P. Berenger in *Actes du Colloque CEM*, (Tregastel, France), 1983.

[12] C. Cerjan, D. Kosloff, R. Kosloff, and M. Reshef, "A nonreflecting boundary condition for discrete acoustic and elastic wave equations," *Geophysics*, vol. 50, pp. 705–708, 1985.

[13] R. Kosloff and D. Kosloff, "Absorbing boundaries for wave propagation

problems," *J. Computational Physics*, vol. 63, pp. 363–376, 1986.

[14] C. M. Rappaport and L. Bahrmasel, "An absorbing boundary condition based on anechoic absorber for EM scattering computation," *J. Electromag. Waves Appl.*, vol. 6, no. 12, pp. 1621–1634, 1992.

[15] J.-P. Berenger, "A perfectly matched layer for the absorption of electromagnetic waves," *J. Computational Physics*, pp. 10-41, March 1994.

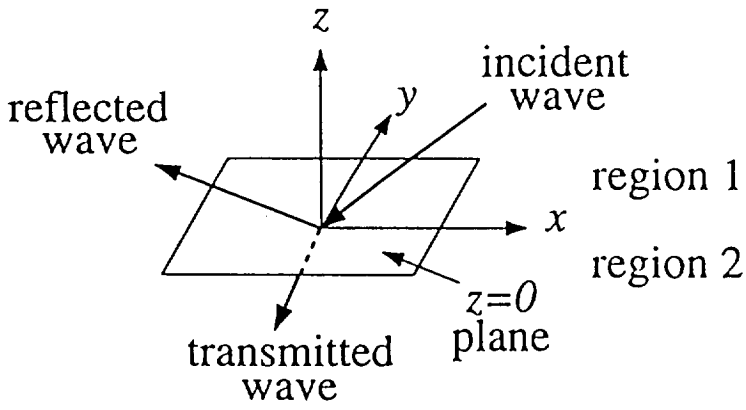

Figure 1. Plane wave with arbitrary polarization incident on the plane $z = 0$.

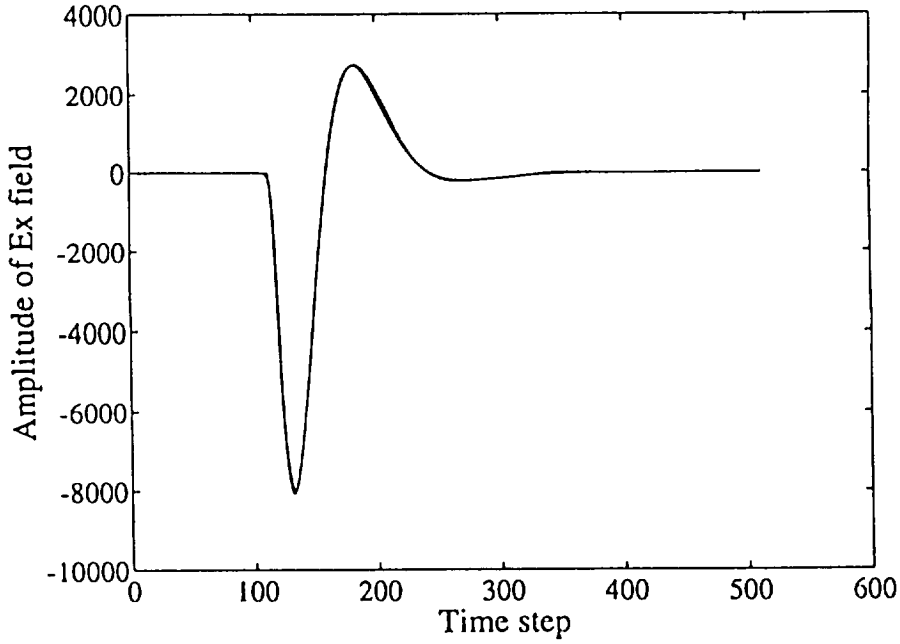

Figure 2. Analytic and numerical FDTD solution overlaid for the E_x field resulting from an infinitesimal electric dipole.

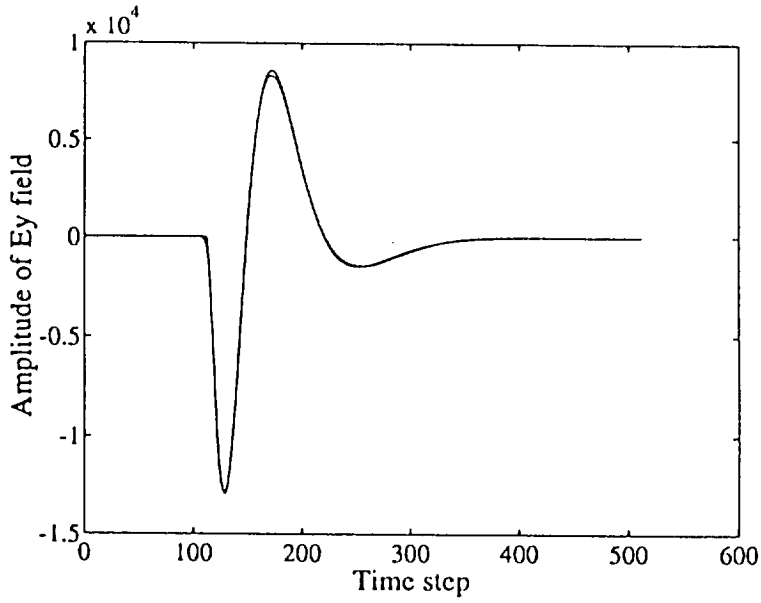

Figure 3. Analytic and numerical FDTD solution overlaid for the E_y field resulting from an infinitesimal electric dipole.

Nodes	CPU sec (Run 1, Run 2, Run 3, Avg.)
32	50.5, 50.2, 50.6; 50.4
64	29.9, 30.0, 30.0; 30.0
128	17.9, 18.4, 18.4; 18.2
256	12.4, 13.2, 12.7; 12.8

Table 1. CPU times for FDTD Problem on CM-5.

CHAPTER 3

FAST MULTIPOLE METHOD SOLUTION USING PARAMETRIC GEOMETRY

1. Introduction

Practical electromagnetic problems are often three-dimensional (3-D) and involve arbitrary geometry. In the case when an object of curvature is of interest, the use of flat facets creates unnecessary artificial discretization in the solution. Recently, many researchers have been investigating the use of curved patches [1-3]. Wilkes and Cha [2] extended the flat triangular patch moment method solution developed by Rao, Wilton, and Glisson [4] to the curved triangular patch. This part presents a technique for computing the electromagnetic radiation and scattering from 3-D conducting bodies of general shape. The arbitrary surface is described by dividing it into a number of connected patches which are mathematically described as parametric quadratic surfaces. The electric field integral equation (EFIE) is solved by standard MOM technique with specifically designed basic functions for subdomains which now contain surface curvature.

2. Parametric Quadratic Surface Description

An arbitrary surface with curvature can generally be represented using two parameters: $u_1$and u_2. The surface is then described by the equation $\mathbf{r}(u_1, u_2)$. A differential tangent vector is given by

$$d\mathbf{r} = \frac{\partial \mathbf{r}}{\partial u_1} du_1 + \frac{\partial \mathbf{r}}{\partial u_2} du_2 \tag{1}$$

Any vector tangential to the surface can be written as a linear combination of $\frac{\partial \mathbf{r}}{\partial u_1}$and $\frac{\partial \mathbf{r}}{\partial u_2}$. Generally, the surface is composed of curvilinear patches. These patches are smoothly connected to each other at common boundaries. In this research, $\mathbf{r}(u_1, u_2)$ is a second-order polynomial of $u_1$and u_2. Thus, nine points on each patch should be known with respect to the origin of a known coordinate system. The vector from the origin to the surface of the p-th patch may be written as

$$\mathbf{r}_p(u_1, u_2) = \sum_{m=1}^{3} \sum_{n=1}^{3} C_{mn}^{(p)} u_1^{m-1} u_2^{n-1} \tag{2}$$

for u_1 from 0 to 1, u_2 from 0 to 1, where $C_{mn}^{(p)}$ are related to the known nine points coordinates, and can be solved from the following linear equations

$$\begin{aligned} \mathbf{r}_p(0,0) &= \mathbf{r}_{11} \\ \mathbf{r}_p(0,0.5) &= \mathbf{r}_{12} \\ \mathbf{r}_p(0,1) &= \mathbf{r}_{13} \\ \mathbf{r}_p(0.5,0) &= \mathbf{r}_{21} \\ \mathbf{r}_p(0.5,0.5) &= \mathbf{r}_{22} \\ \mathbf{r}_p(0.5,1) &= \mathbf{r}_{23} \\ \mathbf{r}_p(1,0) &= \mathbf{r}_{31} \\ \mathbf{r}_p(1,0.5) &= \mathbf{r}_{32} \\ \mathbf{r}_p(1,1) &= \mathbf{r}_{33} \end{aligned} \tag{3}$$

3. MOM Solutions

For conducting objects, the EFIE is given by

$$\widehat{t} \cdot \int_S \left[\mathbf{J}(\mathbf{r}') + \frac{1}{k^2} \nabla' \cdot \mathbf{J}(\mathbf{r}') \nabla \right] \frac{e^{ikR}}{R} dS' = \frac{4\pi i}{k\eta} \widehat{t} \cdot \mathbf{E}^i(\mathbf{r}) \tag{4}$$

for $\mathbf{r}$ on surface S, where $\widehat{t}$ is any unit tangent vector on S, $\mathbf{E}^i$ is an impressed field which excites system, and it is isolated in an impressed field region, or an incident plane wave, and $R = |\mathbf{r} - \mathbf{r}'|$.

The EFIE for the unknown electric current on the conducting surface induced by an incident wave is solved using standard Method of Moments (MOM) technique. Each patch is segmented into quadrilateral cells (in parametric space, these cells are rectangular). The unknown current $\mathbf{J}(\mathbf{r})$ is first expanded in an appropriately chosen set of basis functions $\{\mathbf{j}_{u_{1m}}\}$ and $\{\mathbf{j}_{u_{2m}}\}$

$$\mathbf{J}(\mathbf{r}) = \sum_{\alpha=u_1,u_2} \sum_{n=1}^{N} a_{\alpha n} \mathbf{j}_{\alpha n}(\mathbf{r}) \tag{5}$$

where $a_{\alpha n}$ are the unknown expansion coefficients. The basis functions used lie on the surface of a pair of curved quadrilateral cells is defined as

$$\mathbf{j}_{u_{1m}} = \sqrt{\frac{g_{22}(u_{1m},u_{2m})}{g(u_1,u_2)}} T_{u_{1m}}(u_1) P_{u_{2m}}(u_2) \frac{\partial \mathbf{r}}{\partial u_1} \tag{6}$$

$$\mathbf{j}_{u_{2m}} = \sqrt{\frac{g_{11}(u_{1m},u_{2m})}{g(u_1,u_2)}} T_{u_{2m}}(u_2) P_{u_{21m}}(u_1) \frac{\partial \mathbf{r}}{\partial u_2} \tag{7}$$

where T_u is a triangular function, P_u is a pulse function, and

$$g_{ij} = \frac{\partial \mathbf{r}}{\partial u_i} \cdot \frac{\partial \mathbf{r}}{\partial u_j} \tag{8}$$

is known as the metric tensor. In differential geometry, it is often called the first principal form. The determinant of g_{ij} is

$$g = g_{11}g_{22} - g_{12}^2. \tag{9}$$

It can be proved that the divergences of basis functions are finite, and thus there are no artificial line charges on the patch. Furthermore, as the patch dimension becomes small compared to the radius of curvature, this basis function approaches the rooftop function for flat patches. Since currents flow across the junctions of connected patches, an additional set of overlap modes has been added to the usual expansions [5].

The EFIE for $\mathbf{J}(\mathbf{r})$ is discretized by substituting the above expansion in terms of unknowns $a_{\alpha n}$. Then, rather than forcing the EFIE to be satisfied for $\mathbf{r}$ on surface S, it is tested with integration along a line from the center of a cell to the center of adjacent cell (line matching), and with the same basis functions (Galerkins method).

Usually the most important and difficult to evaluate terms in MOM matrix are the self impedance terms since the Green function contains an integrable singularity at $|\mathbf{r} - \mathbf{r}'|$. The procedure used to treat these singularities is to add and subtract a singular term from the integrals which can be integrated analytically and also renders the integrals well behaved so that standard numerical integration methods can be applied. The scalar potential integral can be written as

$$\int\int \frac{e^{ikR}}{R}\, du_1' du_2' = \int\int \left[\frac{e^{ikR}}{R} - \frac{1}{R_0}\right] du_1' du_2' + \int\int \frac{du_1' du_2'}{R_0}. \tag{10}$$

The function R_0, which should have the same behavior as near the singularity, is developed by using a Taylor series approximation of $\mathbf{r}'$ near $\mathbf{r}$. Thus R_0 is defined as

$$R_0 = \sqrt{g_{11}\left(u_1' - u_1\right)^2 + g_{22}\left(u_2' - u_2\right)^2 + 2g_{12}\left(u_1' - u_1\right)\left(u_1' - u_1\right)} \tag{10a}$$

Then the integral of $1/R_0$ can be found analytically.

4. The Fast Multipole Algorithm

As can be seen, the scattering by arbitrarily shape of conductor can be converted to finding the solutions of an integral equation where the unknown

function is the induced current distribution. The integral equation can be converted to a matrix equation by the method of moments (MOM). The resultant matrix equation is then solved by Gaussian elimination, which requires $O(N^3)$ floating-operations if Gaussian elimination is used to solve N linear equations, or $O(N^2)$ operations per iteration if the conjugate gradient (CG) method is used.

The fast multipole method (FMM) [6,7] is designed to speed up the matrix-vector multiply in the CG method when it is used to solve the matrix equation. The idea is first to divide the subscatters into groups. Then, addition theorem [8] is used to translate the scattered field of different scattering centers within a group into a single center. Hence, the number of scattering centers is reduced. Similarly, for each group, the field scattered by all the other group centers can be first "received" by the group center, and then "redistributed" to the subscatterers belonging to the group.

The addition theorem [8,9] has the form

$$\frac{e^{ik|\mathbf{x}+\mathbf{d}|}}{|\mathbf{x}+\mathbf{d}|} = ik\sum_{l=0}^{\infty}(-1)^l(2l+1)j_l(kd)h_l^{(1)}(kx)P_l(\hat{d}\cdot\hat{x}) \tag{11}$$

where j_l is a spherical Bessel function of the first kind, $h_l^{(1)}$ is a spherical Hankel function of the first kind, P_l is a Legendre polynomial, and $d < x$.

Substituting the elementary identity [10, p. 410]

$$4\pi i^l j_l(kd)P_l(\hat{d}\cdot\hat{x}) = \int d^2\hat{k}e^{i\mathbf{k}\cdot\mathbf{d}}P_l(\hat{k}\cdot\hat{x}) \tag{12}$$

into Equation (1) yields

$$\frac{e^{ik|\mathbf{x}+\mathbf{d}|}}{|\mathbf{x}+\mathbf{d}|} = \frac{ik}{4\pi}\int d^2\hat{k}e^{i\mathbf{k}\cdot\mathbf{d}}\sum_{l=0}^{\infty} i^l(2l+1)h_l^{(1)}(kx)P_l(\hat{k}\cdot\hat{x}) \tag{13}$$

$$\approx \frac{ik}{4\pi}\int d^2\hat{k}e^{i\mathbf{k}\cdot\mathbf{d}}T_L(\cos\theta). \tag{14}$$

We have truncated the sum of infinite series, where $\int d^2\hat{k}$ represents the integrals over the unit sphere, and

$$T_l(\cos\theta) = \sum_{l=0}^{L} i^l(2l+1)h_l^{(1)}(kx)P_l(\cos\theta). \tag{15}$$

Letting $\mathbf{r}_j$ and $\mathbf{r}_i$ be the field point and source point, respectively, we have

$$\begin{aligned}\mathbf{r}_{ji} = \mathbf{r}_j - \mathbf{r}_i &= \mathbf{r}_j - \mathbf{r}_m + \mathbf{r}_m - \mathbf{r}'_m + \mathbf{r}'_m - \mathbf{r}_i \\ &= \mathbf{r}_{jm} + \mathbf{r}_{mm'} - \mathbf{r}_{im'}.\end{aligned} \tag{16}$$

Thus, the scalar Green's function can be rewritten as

$$\frac{e^{ikr_{ji}}}{r_{ji}} = \frac{ik}{4\pi}\int d^2\hat{k}e^{i\mathbf{k}\cdot(\mathbf{r}_{jm}-\mathbf{r}_{im'})} \quad \alpha_{mm'}(\hat{r}_{mm'}\cdot\hat{k}) \tag{17}$$

where

$$\alpha_{mm'}(\hat{r}_{mm'}\cdot\hat{k}) = \sum_{l=0}^{L} i^l(2l+1)h_l^{(1)}(kr_{mm'})P_l(\hat{r}_{mm'}\cdot\hat{k}). \tag{18}$$

The integration in (17) will be evaluated by Gaussian quadratures with $k = 2L^2$ points.

For conducting objects, the electric field integral equation (EFIE) from (4) is written alternatively as

$$\hat{t}\cdot\int_S \overline{\mathbf{G}}(\mathbf{r},\mathbf{r}')\cdot\mathbf{J}(\mathbf{r}')dS' = \frac{i}{k\eta}\hat{t}\cdot\mathbf{E}^i(\mathbf{r}) \tag{19}$$

where

$$\overline{\mathbf{G}}(\mathbf{r},\mathbf{r}') = \left[\bar{\mathbf{I}} - \frac{1}{k^2}\nabla\nabla'\right]\frac{e^{ikr_{ji}}}{4\pi r_{ji}}. \tag{20}$$

Using the scalar Green's function (7), we get

$$\overline{\mathbf{G}}(\mathbf{r}_j,\mathbf{r}_i) = \frac{ik}{4\pi}\int d^2\hat{k}(\bar{\mathbf{I}} - \hat{k}\hat{k})e^{i\mathbf{k}\cdot(\mathbf{r}_{jm}-\mathbf{r}_{im'})} \quad \alpha_{mm'}(\hat{r}_{mm'}\cdot\hat{k}). \tag{21}$$

Applying MOM to the EFIE with basis function $\mathbf{j}_i$ and testing function $\mathbf{t}_j$, we transform the integral equation to matrix equation

$$\sum_{i=1}^{N} A_{ji}a_i = F_j, \quad j = 1,2,\cdots,N \tag{22}$$

where

$$A_{ji} = \int_S dS\mathbf{t}_j(\mathbf{r})\cdot\int_S' dS'\overline{\mathbf{G}}(\mathbf{r},\mathbf{r}')\cdot\mathbf{j}_i(\mathbf{r}') \tag{23}$$

$$F_j = \frac{1}{k\eta}\int_S dS\mathbf{t}_j(\mathbf{r})\cdot\mathbf{E}^i(\mathbf{r}). \tag{14}$$

For non-nearby group pair (m, m'), Substituting Equation (21) into (23) yields

$$A_{ji} = \frac{ik}{4\pi} \int d^2\hat{k} \mathbf{V}_{fmj}(\hat{k}) \cdot \alpha_{mm'}(\hat{k} \cdot \hat{r}_{mm'}) \mathbf{V}^*_{sm'i}(\hat{k}) \tag{15}$$

where

$$\mathbf{V}_{sm'i}(\hat{k}) = \int ds' e^{i\mathbf{k}\cdot\mathbf{r}_{im'}} [\mathbf{I} - \hat{k}\hat{k}] \cdot \mathbf{j}_i(\mathbf{r}_{im'}) \tag{16}$$

$$\mathbf{V}_{fmj}(\hat{k}) = \int ds' e^{i\mathbf{k}\cdot\mathbf{r}_{jm'}} [\mathbf{I} - \hat{k}\hat{k}] \cdot \mathbf{t}_j(\mathbf{r}_{im}) \tag{17}$$

When $\mathbf{r}_i$ and $\mathbf{t}_j$ are same functions, this is Galerkin's method.

Before solving the matrix equation by CG, we need to calculate some matrix elements. First, we divide the N basis functions into G localized groups, labeled by an index m, each supporting about $M = N/G$ basis functions. Second, for nearby group pairs (m, m'), we calculate the matrix elements by direct numerical computation. Third, we compute $\mathbf{V}_{smi}(\hat{k})$ and $\mathbf{V}_{fmj}(\hat{k})$ for K directions of $\hat{k}$. Finally, we compute $\alpha_{mm'}(\hat{k} \cdot \hat{r}_{mm'})$ for each non-nearby group pair (m, m').

4.1. Algorithm for Matrix-Vector Multiplication by FMM

1.

$$\mathbf{S}_m(\hat{k}) = \sum_{i \in G_m} \mathbf{V}^*_{smi}(\hat{k}) a_i. \tag{18}$$

This step requires $O(KN)$ operations.

2.

$$\mathbf{g}_m(\hat{k}) = \sum_{m'} \alpha_{mm'}(\hat{k} \cdot \hat{r}_{mm'}) \mathbf{S}'_m(\hat{k}). \tag{19}$$

This step requires $O(kG(G - B))$ operations, where B is the average nearby groups.

3.

$$\sum_{i=1}^{N} A_{ji} a_i = \sum_{m'} \sum_{i \in G_{m'}} A_{ji} a_i + \int d^2\hat{k} \mathbf{V}_{fmj}(\hat{k}) \cdot \mathbf{g}_m(\hat{k}), \qquad j \in G_m. \tag{20}$$

The first term is the contribution from nearby groups (including itself), and the second term is the far interaction calculated by FMM. This step requires $O(BGM^2) + O(KN)$ operations.

To ensure that the Green's function to converge to the desired accuracy, we choose

$$L = kD + \ln(\pi + kD) \tag{21}$$

where D is the maximum diameter of a group size. Thus L is proportional to the size D, and K is proportional to the surface area of the group. Since the unknowns in each group (M) is proportional to the surface area too, then $K \sim M$. The computation in the matrix-vector multiply requires $T = C_1NG + C_2N^2/G$ operations, where C_1 and C_2 are machine and implementation dependent. The total operation count is minimized by choosing $G = \sqrt{C_2N/G}$. Therefore, $T = 2\sqrt{C_1C_2}N^{1.5}$.

5. Ray Propagatin Fast Multipole Algorithm (RPFMA)

In the above, $\alpha_{mm'}(\hat{k} \cdot \hat{r}_{mm'})$ translates the field radiated from a transmitting group in some dirction $\hat{k}$ into the received component in the same direction at a receiving group. We expect the interation to be strongest for fields radiated along the line joining the transmitting and receiving groups. Thus, we can ignore some $\hat{k}$'s when $\alpha_{mm'}(\hat{k} \cdot \hat{r}_{mm'})$ is too small compared to the maximum of $\alpha_{mm'}(\hat{k} \cdot \hat{r}_{mm'})$. To take full advantage of this idea, we use a window function in the calculation of $\alpha_{mm'}(\hat{k} \cdot \hat{r}_{mm'})$ (Equation (18) is a Fourier series computed with a square window in the variable l). Thus, denoting the window function W_l, the elements of $\alpha_{mm'}(\hat{k} \cdot \hat{r}_{mm'})$ are calculated as

$$\alpha_{mm'}(\hat{k} \cdot \hat{r}_{mm'}) = \sum_{l=0}^{L} W_l i^l (2l + l) h_l^{(1)}(kr_{mm'}) P_l(\hat{k} \cdot \hat{r}_{mm'}). \tag{22}$$

Using this ray propagation idea, the cost of step 2 is reduced from KG^2 to K_0G^2, where K_0 is independent of group size. The total operations of a RPFMA matrix-vector multiplication become

$$T = C_3G^2 + C_2N^2/G. \tag{23}$$

It is minimized when $G \sim N^{2/3}$, Therefore $T \sim N^{4/3}$.

6. Numerical Results

Numerical implementations are verified by comparing the results with some known ones in published papers for a conducting plate with different shape (square, rectangular, triangular, disk, etc.). The program is tested on the case of a conducting sphere since it is one of the very few cases for which accurate and comprehensive data are available. Compared with Mie series, the bistatic Radar Cross Section (RCS) using curved quadrilateral patches is as good as using curved triangular patches [2]. The latter uses more input geometry data.

The RCS of a 14 inches NASA Almond is calculated at $f = 2\,\text{GHz}$. The results agree with the experimental and numerical results given by Newman [5].

The fast multiple method has also been implemented. Figure 2a shows the comparison of the CPU time versus the number of unknowns for the fast multipole method (FMM), the ray-propagation fast multipole algorithm (RPFMA), standard CG, and LU decomposition for calculating the bistatic RCS of a square metallic plate at normal incidence. The plate is discretized with 10 unknowns per wavelength. It is seen that the FMM and RPFMA both outperform the standard CG in terms of matrix fill and matrix solve. The FMM and RPFMA also require less memory, and hence, can solve a larger problem on a small computer. The simulation is performed on a SUN-SPARC-2 with 64 MB of RAM. Figure 2b shows a similar plot for a conducting sphere.

Figure 3 shows the validation of the FMM with the Mie series solution for the bistatic RCS of a conducting sphere of radius 1 m and at frequency of 0.42 GHz for the parallel polorization. Ten unknowns are used per wavelength.

Figure 4 shows the RCS of a wedge cylinder with plate extension having a total length of 3.73 m, and width of 2 m at 0.3 GHz. The plate is in the xy plane while the wave is incident at 80° from normal. The computation is done with LU decompostion requiring 2.5 hr of CPU time on a SUN-SPARC-2. Some points computed with FMM are shown, but it took FMM 0.5 hr/point in these computations.

Figure 5 shows the RCS of a one meter long NASA almond at 2.5 GHz in the xy plane with $\theta = 90°$. Five unknowns are used per wavelength. The calculation is done with LU decomposition on a SUN-SPARC-10 with 128 MB RAM, and it consumes about 24 hr of CPU time. Some points computed with FMM are shown. These points took 3 hr/point to compute.

In summary, we describe the arbitrary shape of conducting body using curved patch. The EFIE is discretized by MOM with rooftop basis functions. Numerical results agree very well with those of existing studies. This approach needs less unknowns since it describes the object more accurately.

We have compared various method of solving the resultant dense matrix equation: using LU decomposition, fast multipole method, and the ray-propagation fast multipole algorithm. For one bistatic RCS involving one incident angle, FMM and RPFMA outperform LU decomposition when the number of unknowns is more than 2,000. RPFMA only performs marginally better than FMM because the problem size we have been able to run is not large enough.

For monostatic RCS involving many incident angles, FMM and RPFMA

does not show an advantage over LU decomposition. To have an advantage, the number of iterations in FMM and RPFMA will have to be reduced, and their computational complexity has to be further reduced.

References

[1] M. I. Sancer, R. L. McClary, and K. J. Glover,"Electromagnetic Computation Using Parametric Geometry," *J. of Electromagnetic Waves and Applications*, vol. 10, pp. 85-103, 1990.

[2] D. L. Wilkes and C. -C. Cha, "Method of Moments Solution with Parametric Curved Triangular Patches," *1991 International IEEE AP-S Symposium Digest*, pp. 1512-1515, London, Ontario, Canada, 1991.

[3] S. Wandzura, "Electric Current Basis Functions for Curved Surfaces," *J. of Electromagnetic Waves and Applications*, vol. 12, pp. 77-91, 1992.

[4] S. M. Rao, D. R. Wilton, and A. W. Glisson, "Electromagnetic Scattering by Surfaces of Arbitrary Shape," *IEEE Transactions on Antenna and Propagation*, pp. 409-418, 1982.

[5] E. H. Newman, "Polygonal Plate Modeling," *J. of Electromagnetic Waves and Applications*, vol.10, pp. 65-83, 1990.

[6] V. Rokhlin, "Rapid Solution of Integral Equations of Scattering Theory in Two Dimensions," *J. Comput. Phys*, vol. 36, no. 2, pp. 414-439, February 1990.

[7] C.C. Lu and W.C. Chew, "A Fast Algorithm for Solving Hybrid Integral Equation," *IEE Proceedings-H*, vol. 140, no. 6, pp. 455-460, December 1993.

[8] M. Abromowitz and I.A. Stegun, *Handbook of Mathematical Functions,* Dover Publication, New York, 1972.

[9] R. Coifman, V. Rokhlin, and S. Wandzura, "The fast multipole method for the wave equation: A pedestrian prescription," *IEEE Ant. Propag. Mag.*, vol. 35, no. 3, pp. 7-12, June 1993.

[10] J. Stratton, *Electromagnetic Theory,* McGraw-Hill, New York, 1941.

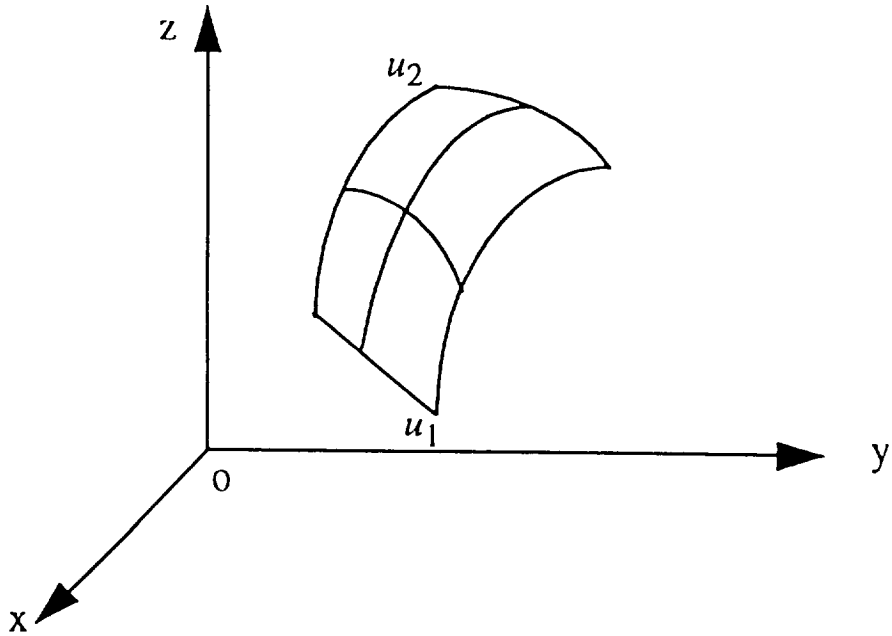

Figure 1. Curved quadrilateral patch defined by nine points.

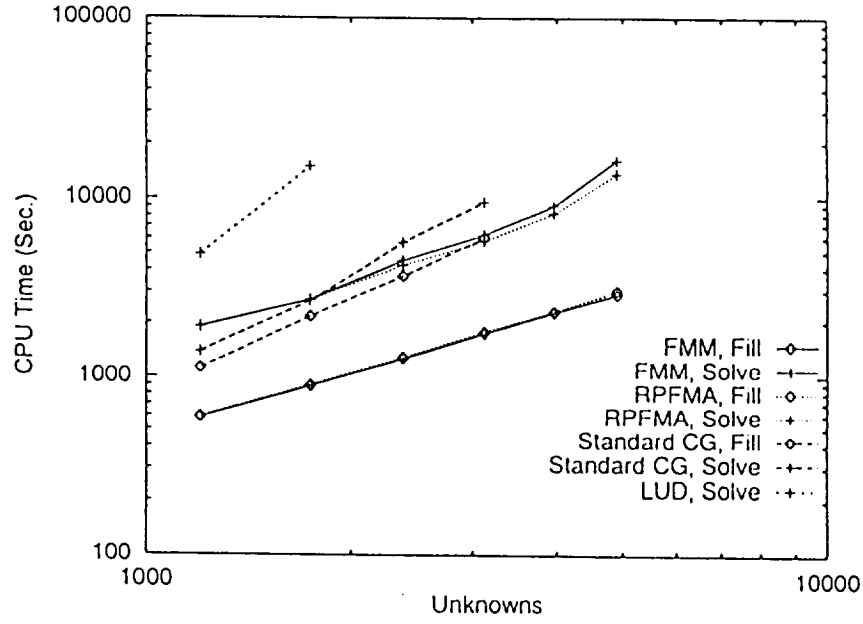

(a)

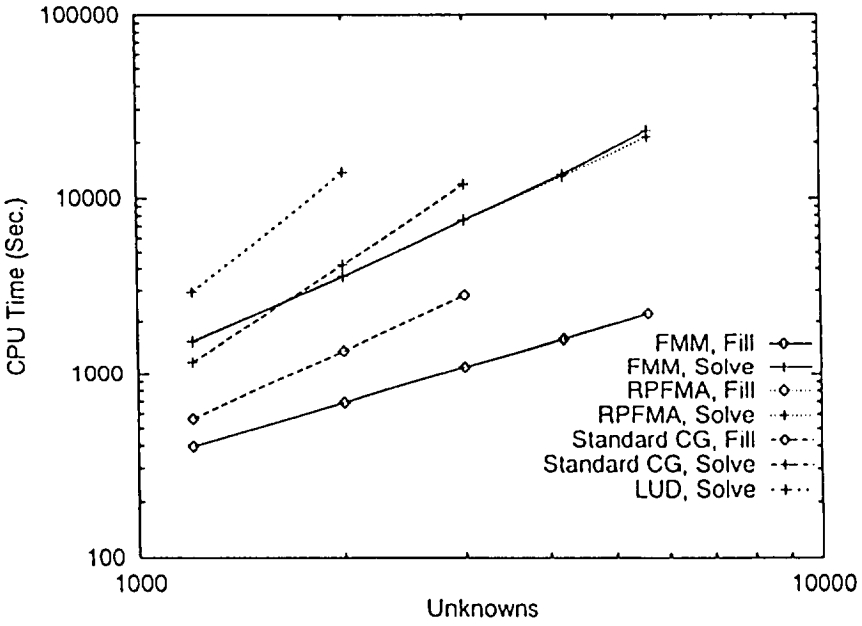

(b)

Figure 2. (a) Comparison of the CPU time versus the number of unknowns for FMM, RPFMA, standard CG and LU decomposition for a square metallic plate. (b) The same as (a) but for a metallic sphere.

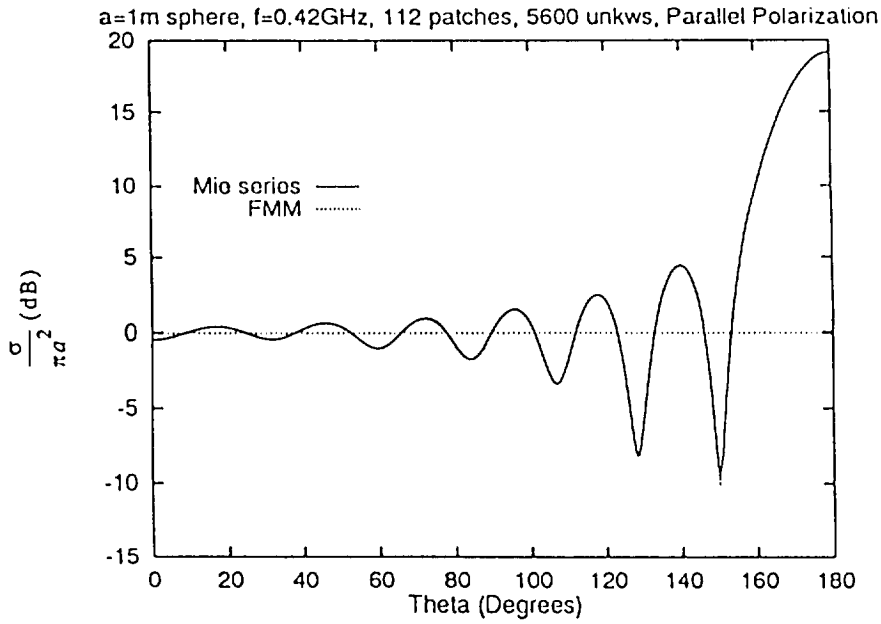

Figure 3. Validation of FMM against the Mie series solution of the bistatic RCS of a conducting sphere of radius 1 m at 0.42 GHz. Ten unknowns are used per wavelength.

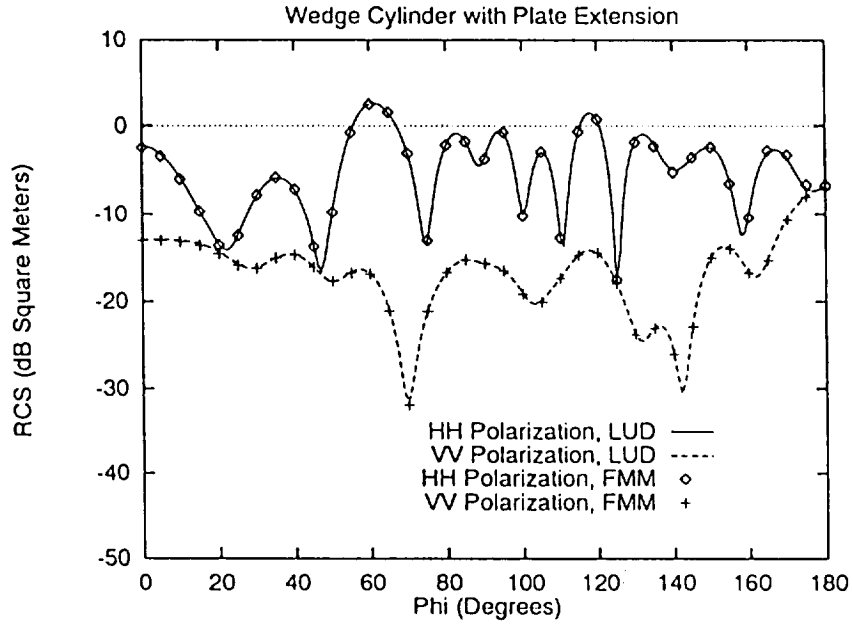

Figure 4. RCS of a wedge cylinder with plate extension from a NASA test case. The results are computed with LU decomposition, and partially with FMM.

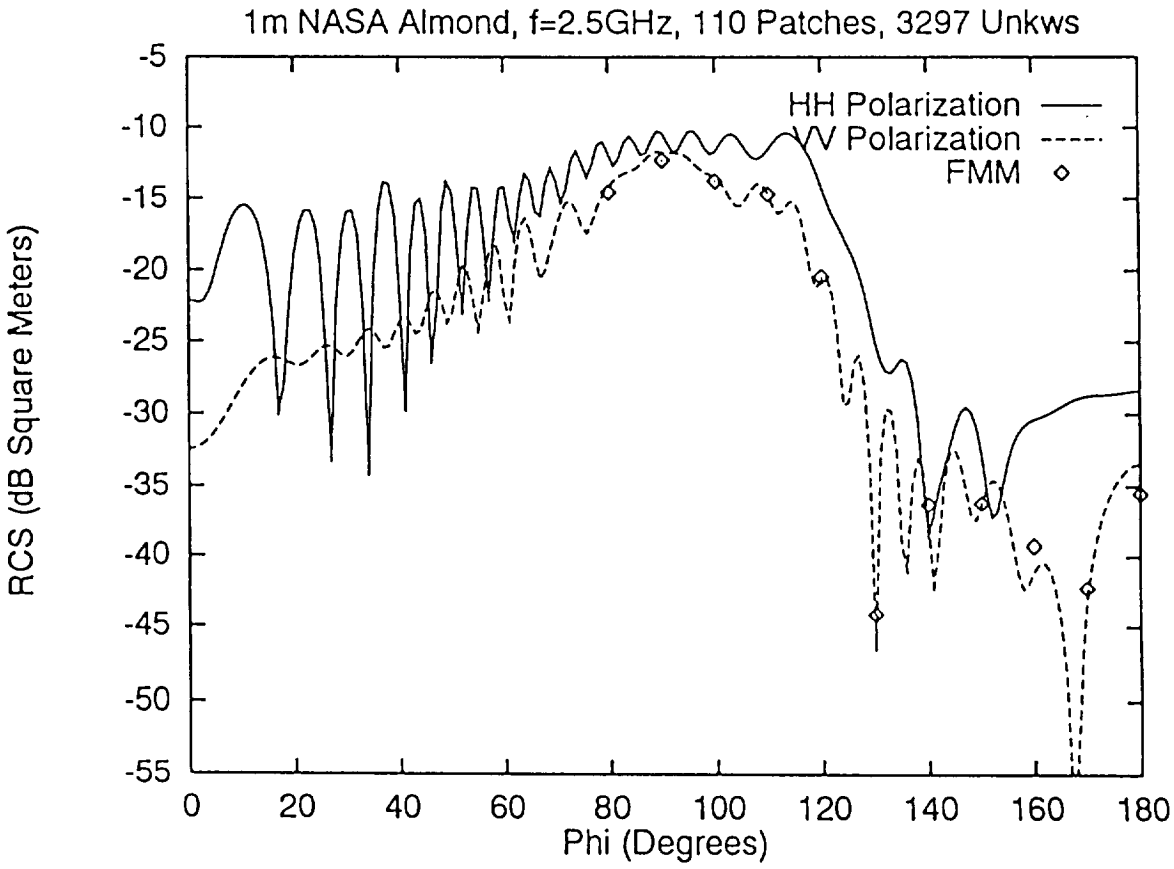

Figure 5. RCS of a one-meter long NASA almond at 2.5 GHz in the xy plane with $\theta = 90°$. Five unknowns are used per wavelength. The results are computed with LU decomposition, and partially with FMM.